nature cell biology

Competition amongst Eph receptors regulates contact inhibition of locomotion and invasiveness in prostate cancer cells

Jonathan W. Astin[1], Jennifer Batson[1], Shereen Kadir[1], Jessica Charlet[1], Raj A. Persad[3], David Gillatt[3], Jon D. Oxley[4] and Catherine D. Nobes[1,2,5]

Metastatic cancer cells typically fail to halt migration on contact with non-cancer cells. This invasiveness is in contrast to normal mesenchymal cells that retract on contact with another cell. Why cancer cells are defective in contact inhibition of locomotion is not understood. Here, we analyse the dynamics of prostate cancer cell lines co-cultured with fibroblasts, and demonstrate that a combinatorial code of Eph receptor activation dictates whether cell migration will be contact inhibited. The unimpeded migration of metastatic PC-3 cells towards fibroblasts is dependent on activation of EphB3 and EphB4 by ephrin-B2, which we show activates Cdc42 and cell migration. Knockdown of EphB3 and EphB4 restores contact inhibition of locomotion to PC-3 cells. Conversely, homotypic collisions between two cancer cells results in contact inhibition of locomotion, mediated by EphA–Rho–Rho kinase (ROCK) signalling. Thus, the migration of cancer cells can switch from restrained to invasive, depending on the Eph-receptor profile of the cancer cell and the reciprocal ephrin ligands expressed by neighbouring cells.

Over 30 years ago, whilst investigating the phenomenon of contact inhibition of locomotion (CIL)—a process defined as "the stopping of the continual locomotion of a cell in the same direction after collision with another cell"[1]—it was noted that many metastatic cancer cells demonstrate unimpeded migration when they come into contact with non-malignant cells[2,3]. Curiously, malignant cells did undergo CIL when contacting one another[3]. It was proposed that these alternate responses might increase metastasis[4,5] because cancer cell dissemination would be enhanced by repulsive interactions between cancer cells, but local invasion would not be impeded, and might even be facilitated, by interactions with stromal cells within and beyond the tumour[6,7]. Although historically studies of CIL were performed *in vitro*, recent work has shown that these events also occur *in vivo*[8,9]. However, investigating the role of CIL in cancer cell invasion has not been possible because the molecular cues underlying CIL in human cancer cells have not been identified.

The Eph receptors and their membrane-associated ephrin ligands are potential candidates for regulators of CIL. They are activated by cell–cell contact and control cell movements by regulating the actin cytoskeleton. They bind ephrin ligands, which are subdivided into two classes: the GPI (glycosylphosphatidylinositol)-linked ephrin-A ligands and the transmembrane ephrin-B ligands. Eph receptors are also separated into either EphA or EphB subclasses based, in part, on their affinity for either ephrin-A or ephrin-B ligands. Eph–ephrin signalling has a key role in many developmental processes, including axon guidance, angiogenesis and tissue-boundary formation[10–12]. The engagement of surface ephrin ligands on one cell with Eph receptors on another cell activates bi-directional signalling in both ligand- and receptor-expressing cells[13]. The consequent downstream pathways have been shown to regulate cell motility, cell adhesion and cell polarity and are mediated, in particular, by Rho family GTPases[14]. More recently, the mis-expression of various members of the Eph/ephrin family has been associated with carcinoma development, including in the colon, breast and prostate[15,16].

In this study, we characterise the molecular mechanisms that underpin why some cancer cells have defective CIL. We find that CIL between prostate cancer cells is mediated by EphA signalling. However, PC-3 prostate cancer cells have defective CIL when they collide with fibroblasts or endothelial cells, which we find is because of the elevated levels of EphB3 and EphB4 in PC-3 cells. We demonstrate that an integrated response to both repulsive EphA and attractive EphB signalling pathways dictates whether a cancer cell displays CIL.

RESULTS

PC-3 cells do not display CIL on contact with fibroblasts and endothelial cells

To investigate cancer cell CIL, we used classic CIL experiments, but with human cancer cell lines that are motile in the presence of hepatocyte

[1]School of Biochemistry, University of Bristol, Bristol, BS8 1TD, UK. [2]School of Physiology and Pharmacology, University of Bristol, Bristol, BS8 1TD, UK. [3]Bristol Urological Institute, Southmead Hospital, Bristol, BS10 5NB, UK. [4]Department of Cellular Pathology, Southmead Hospital, Bristol, BS10 5NB, UK.
[5]Correspondence should be addressed to C.D.N (e-mail: Catherine.Nobes@bristol.ac.uk)

Received 08 February 2010; accepted 23 September 2010; published online 14 November 2010; DOI: 10.1038/ncb2122

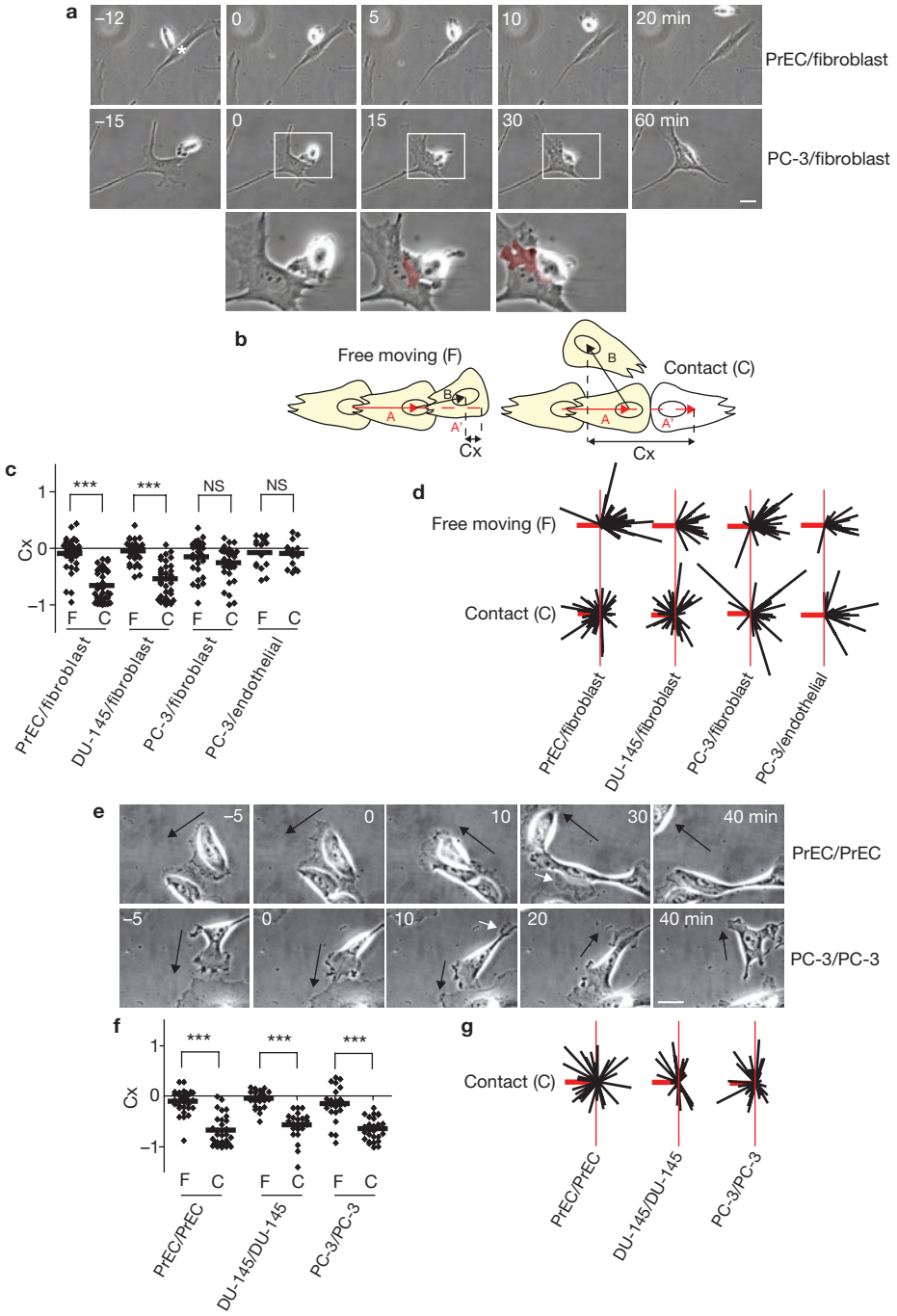

Figure 1 Failure of CIL by PC-3 cells on contact with fibroblasts. (**a**) Representative time-lapse microscopy images, at the indicated times, of a PrEC/fibroblast collision (top and Supplementary Information, Movie S1) and a PC-3/fibroblast collision (middle and Supplementary Information, Movie S2). Asterisk indicates fibroblast cell and insets at the bottom indicate magnification of boxed area; false-colour indicates region of PC-3 cell lamella extending beneath the fibroblast. (**b**) CIL is quantified by comparing contact acceleration indices (Cx) of free-moving cells and colliding cells. Cells were tracked before (A) and after (B) a collision (free-moving cells were tracked for the same time periods). The component Cx of vector B–A represents the difference between how far the cell has progressed in the direction of A' and how far it would have gone had there been no collision. (**c**) Contact acceleration indices (Cx) of free-moving cells (F) versus colliding cells (C); PrEC/fibroblast ($n = 36$), DU-145/fibroblast ($n = 32$), PC-3/fibroblast ($n = 29$), PC-3/endothelial cell ($n = 15$). Triple-asterisks indicate $P < 0.001$, NS; not significant, determined by a Mann-Whitney test. (**d**) Scaled cell-displacement vector diagrams of free-moving cells and colliding cells, tracked during time-lapse microscopy. Thick red line denotes the scaled displacement of all cells before contact and thin black lines are those of each cell following contact. (**e**) Representative time-lapse microscopy images, at the indicated times, of collisions between two PrECs (top and Supplementary Information, Movie S3) and two PC-3 cells (bottom and Supplementary Information, Movie S4). Black arrows indicate direction of migration and white arrow indicates a new leading edge forming. (**f**) Contact acceleration indices (Cx) of free-moving cells (F) versus colliding cells (C); PrEC/PrEC ($n = 31$), DU-145/DU145 ($n = 24$), PC-3/PC-3 ($n = 27$). Triple asterisks indicate $P < 0.001$, determined by a Mann-Whitney test. (**g**) Scaled cell-displacement vector diagrams of homotypic collisions. Cells were tracked during time-lapse microscopy. Thick red line denotes the scaled displacement of all cells before contact and thin black lines are those of each cell following contact. Scale bars: **a**, 50 μm; **e**, 25 μm.

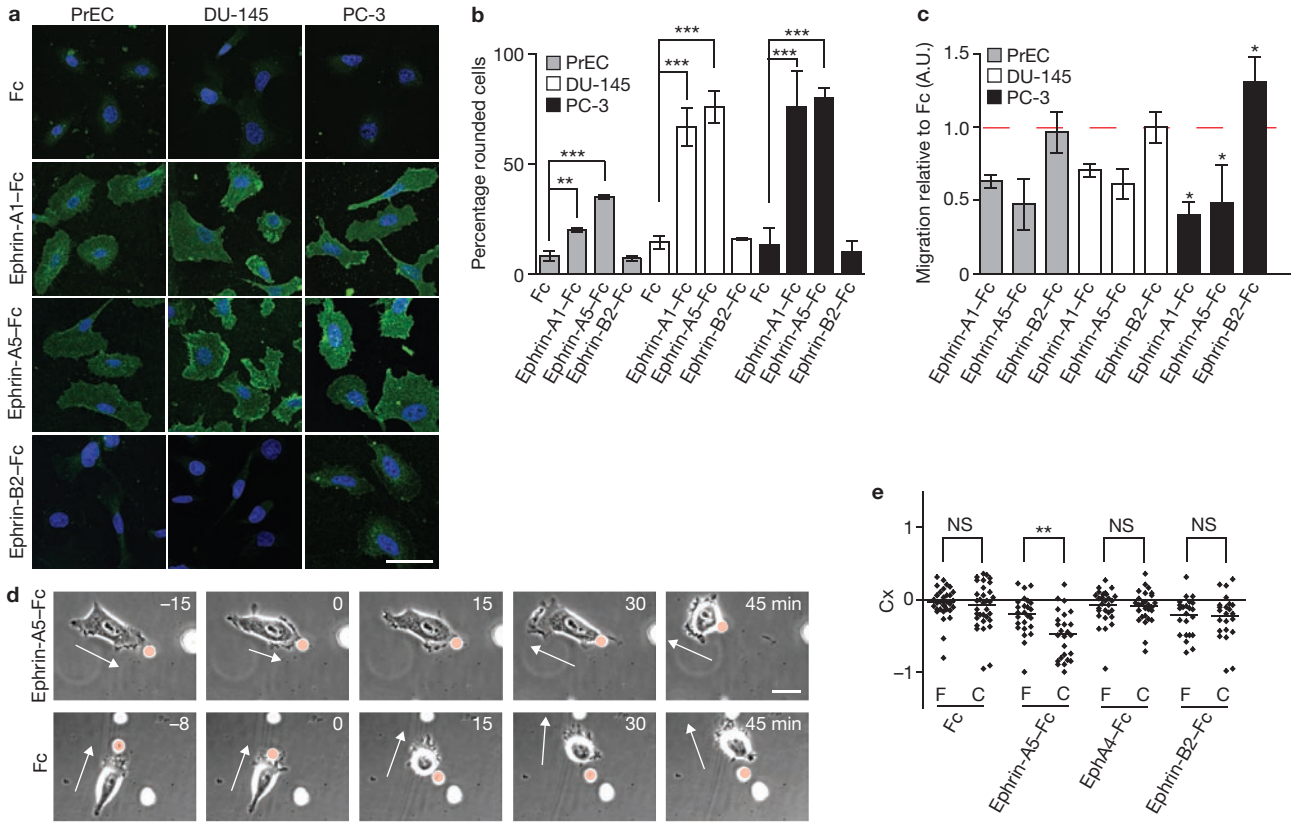

Figure 2 Ephrin-A ligands are sufficient to induce CIL between PC-3 cells. (**a**) Immunofluorescence microscopy of cells treated with anti-Fc antibodies (green) to detect surface binding of ephrin-A1–Fc, ephrin-A5–Fc, ephrin-B2–Fc and control Fc, to PrEC, DU-145 and PC-3 cells. Hoechst (blue) stains nuclei. Scale bar, 50 μm. (**b**) Prostate cells were treated with clustered ephrin–Fc proteins before fixation and phalloidin staining. Data are expressed as percentage of cells with retraction of the cell periphery (rounded cells) for each treatment as indicated. Data are means ± s.d. Triple asterisks indicate $P < 0.001$ and double asterisks indicate $P < 0.01$, as determined by an unpaired Student's *t*-test ($n = 4$; 100 cells counted per experiment). (**c**) The underside of a transwell chamber was coated with ephrin–Fc proteins, as indicated, and the numbers of cells migrating through were scored. Data are expressed as fold-change with respect to control Fc-coated chambers (red dotted line). Data are means ± s.d. Asterisk indicates $P < 0.05$, as determined by a paired Student's *t*-test ($n = 5$). A.U.; arbitrary units. (**d**) Representative time-lapse microscopy images, at the indicated times, of a PC-3 cell colliding with a silica protein-A bead (red pseudocolour) coated with ephrin-A5–Fc (top and Supplementary Information, Movie S5) or with Fc (bottom and Supplementary Information, Movie S6). Arrows indicate direction of migration. Scale bar, 25 μm. (**e**) Contact acceleration indices (Cx) of free-moving cells (F) versus cells colliding with beads (C), coated as indicated; Fc ($n = 33$), ephrin-A5–Fc ($n = 25$), EphA4–Fc ($n = 28$), ephrin-B2–Fc ($n = 23$). Double asterisks indicate $P < 0.01$, as determined by a Mann-Whitney test.

growth factor (HGF). Two frequently studied prostate cancer cell lines are DU-145 and PC-3 cells; both are tumourgenic[17,18], but only PC-3 cells are able to form metastases when injected subcutaneously into mice[19]. We compared the invasiveness of these cancer cell lines with that of non-tumorigenic primary prostate epithelial cells (PrECs)[20]. A collagen I invasion assay (Supplementary Information, Fig. S1) confirmed that the PC-3 cells used here had the greatest invasion properties *in vitro*.

We first tested if PC-3, DU-145 and PrEC cells had different CIL dynamics on contact with fibroblasts and endothelial cells in co-culture (heterotypic CIL; Fig. 1a). PrECs and DU-145 cells demonstrated repulsive CIL after contact with fibroblasts (shown for PrECs in Fig. 1a and Supplementary Information, Movie S1). In contrast, PC-3 cells had defective CIL after collision with a fibroblast, and instead invaded the fibroblast substrate space (Fig. 1a and Supplementary Information, Movie S2).

CIL was quantified using a method adapted from a previous study[3]. Cells were tracked before and after collision, and vector analysis was used to indicate how a cell's migration path deviated from a straight line following collision (Fig. 1b). This deviation was represented as a contact acceleration index (Cx). We observed a significant difference in the Cx values for free-moving and PrEC/fibroblast or DU-145/fibroblast collisions, which shows that these prostate cells demonstrate CIL following contact with fibroblasts. No difference between the Cx values of free-moving PC-3 cells and PC-3 cells in collision was observed, indicating that PC-3 cells do not show CIL when coming into contact with fibroblasts (Fig. 1c). The same data are also presented as scaled cell-displacement vector diagrams (Fig. 1d). Similar results were obtained for heterotypic PC-3 cell/bone marrow endothelial cell (BMEC) collisions (Fig. 1c, d), suggesting that migrating PC-3 cells have lost the ability to be halted on contact with a variety of cell types.

PC-3 cells display normal homotypic CIL

Cancer cells that have defective CIL on contact with non-cancer cells, often demonstrate normal repulsion responses to other cancer cells, which is described as homotypic CIL[3]. PC-3 cells, as well as PrEC and DU-145 prostate cell lines, all demonstrated homotypic CIL (Fig. 1e-g and Supplementary Information, Movies S3 and S4). Therefore, PC-3

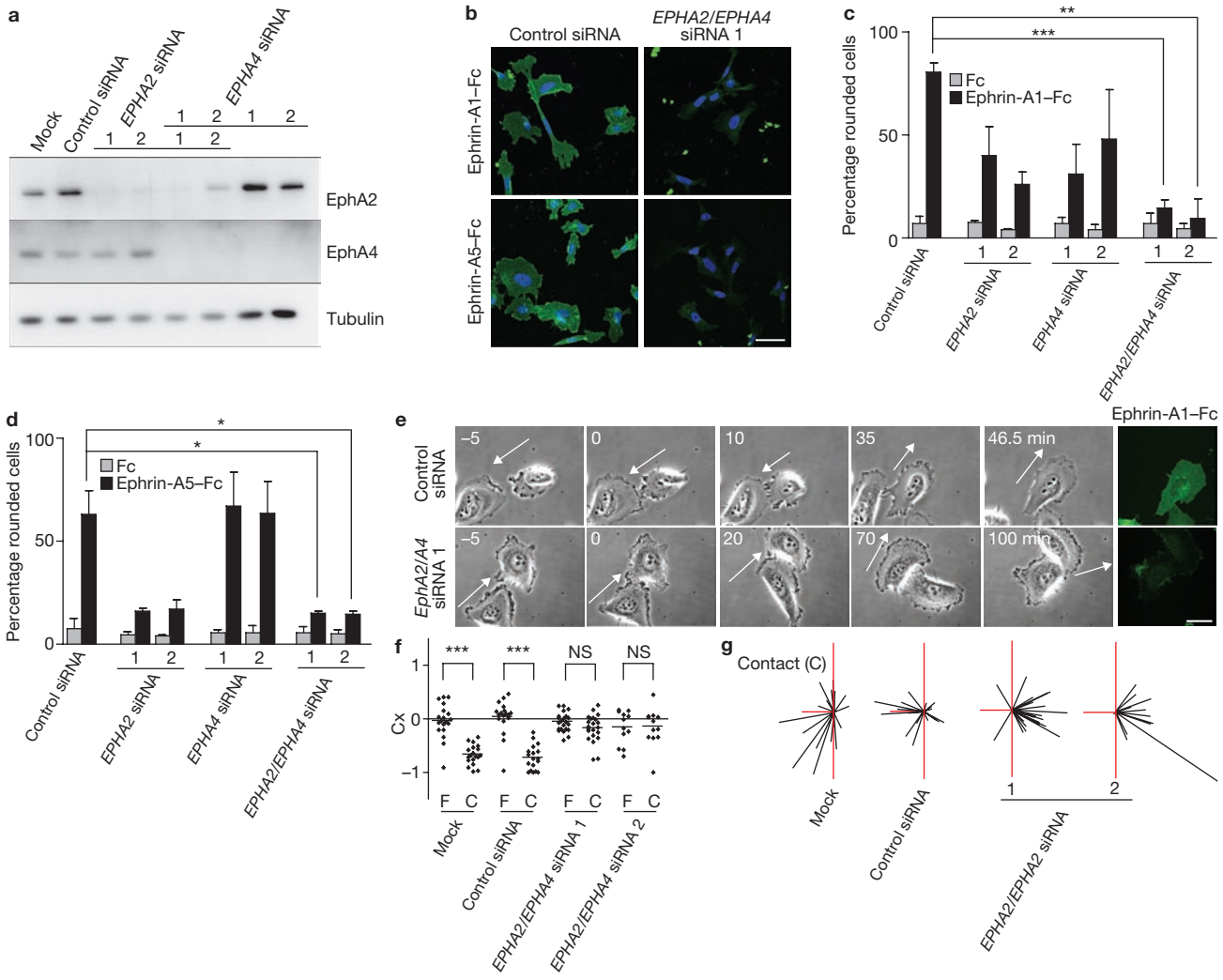

Figure 3 EphA2 and EphA4 are required for CIL between PC-3 cells. (**a**) Lysates of PC-3 cells mock transfected, transfected with a non-targeting siRNA oligonucleotide (control siRNA) or transfected with siRNA oligonucleotides specific to *EPHA2* and *EPHA4* (two different oligonucleotides for each) were immunoblotted using antibodies against the indicated proteins. Tubulin was used as a loading control. (**b**) PC-3 cells transfected with control siRNA or siRNA oligonucleotides specific to *EPHA2* and *EPHA4* were fixed, incubated with either ephrin-A1–Fc (top) or ephrin-A5–Fc (bottom) and stained with anti-Fc antibodies (green) and hoechst (blue). (**c**, **d**) PC-3 cells, transfected with siRNA oligonucleotides as indicated, were treated with clustered ephrin-A1–Fc, ephrin-A5–Fc or Fc, and rounded cells were counted after fixation and staining with phalloidin. Data are means ± s.d. (siRNA 1, $n = 4$; siRNA 2 $n = 3$; 100 cells counted per experiment). Triple asterisks indicate $P < 0.001$, double asterisks indicate $P < 0.01$ and asterisk indicates $P < 0.05$, as determined by an unpaired Student's *t*-test. (**e**) Representative time-lapse microscopy images, at the indicated times, of collisions between PC-3 cells transfected with siRNA oligonucleotides as indicated (Supplementary Information, Movies S7 and S8). Arrows indicate direction of migration. Following time-lapse microscopy, cells were fixed and EphA surface expression of recorded cells was determined by ephrin-A1–Fc binding detected with anti-Fc antibodies (right). (**f**) Contact acceleration indices (Cx) of free-moving (F) versus colliding (C) PC-3 cells transfected with siRNA oligonucleotides as indicated. Mock ($n = 19$), Control ($n = 18$), siRNA 1 ($n = 22$), siRNA 2 ($n = 12$). Triple asterisks indicate $P < 0.001$, NS; not significant, as determined by a Mann-Whitney test. (**g**) Scaled cell-displacement vector diagrams of colliding PC-3 cells treated as shown. Cells were tracked using time-lapse microscopy. Thick red line denotes the scaled displacement of all cells before contact and thin black lines are those of each cell following contact. Scale bars: **b**, 50 μm; **e**, 25 μm. Uncropped images of blots are shown in Supplementary Information, Fig. S8.

cells, similarly to PrECs and DU-145 cells, are capable of homotypic CIL. However, unlike PrECs and DU-145 cells, PC-3 cells do not recognise fibroblasts and endothelial cells as repulsive, possibly because of differences in cell-surface receptors.

Ephrin-A ligands are sufficient to induce CIL in PC-3 cells

Eph receptors and their ephrin ligands regulate cell positioning through direct cell–cell interaction and are probable candidates for mediating CIL responses. Both ephrin-A1 and ephrin-A5 bind to PrECs, DU-145 and PC-3 cells, indicating that all express EphA receptors (Fig. 2a). Detectable surface binding of ephrin-B2 was observed only in PC-3 cells (Fig. 2a), which suggests that these cells have higher expression of EphB. Treatment of PrECs, DU-145 and PC-3 cells with clustered ephrin-A caused rapid activation of RhoA, coupled with ROCK- and actomyosin-mediated retraction of the cell periphery (cell rounding) within 10 min (Fig. 2b and Supplementary Information, Fig. S2), consistent with previous studies[21,22]. Coating Boyden transwell chambers with either ephrin-A1–Fc or ephrin-A5–Fc inhibited the migration of

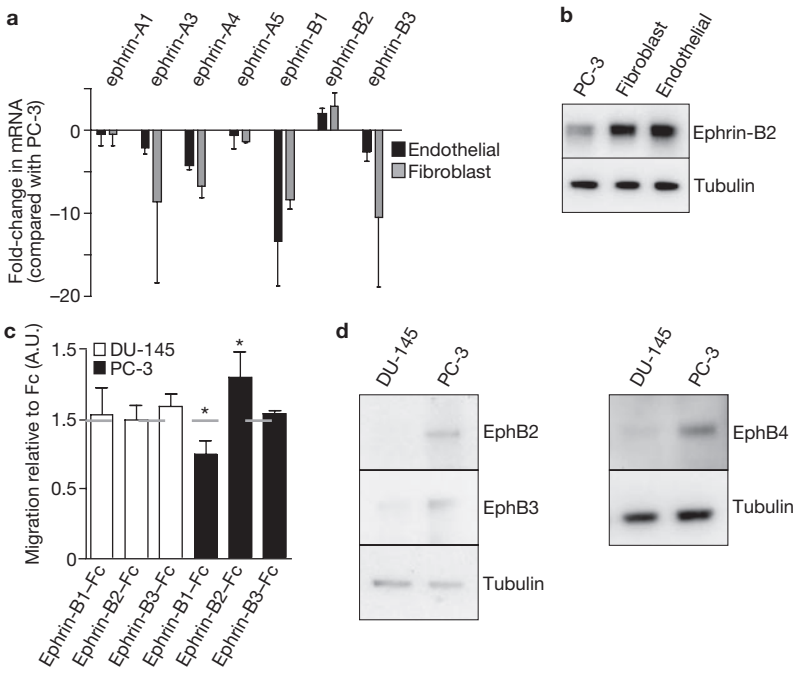

Figure 4 Ephrin-B2 stimulates PC-3 cell migration. (**a**) Relative expression profiles of ephrin ligands by fibroblasts and endothelial cells versus PC-3 cells. Data are expressed as fold-change in mRNA with respect to PC-3 cell mRNA levels, as determined by real-time RT–PCR. Data are means ± s.d. ($n = 3$). (**b**) PC-3, fibroblast and endothelial cell lysates were immunoblotted with antibodies against the indicated proteins. (**c**) The underside of a transwell chamber was coated with Fc-coated ephrin-B-ligands as indicated, and numbers of cells migrating through the chamber were scored. Data are expressed as fold-change with respect to control Fc-coated chambers (grey dotted line). Data are means ± s.d. ($n = 5$). Asterisk indicates $P < 0.05$, as determined by a paired Student's *t*-test. (**d**) Left: EphB2 and EphB3 were immunoprecipitated from lysates of DU-145 or PC-3 cells and detected by immunoblotting. Right: lysates of DU-145 or PC-3 cells were immunoblotted with antibodies against EphB4. Tubulin was used as a loading control in both cases. Uncropped images of blots are shown in Supplementary Information, Fig. S8.

cells, compared with migration of cells in chambers coated with Fc alone (Fig. 2c). In contrast, ephrin-B2–Fc enhanced migration of PC-3 cells in this assay (Fig. 2c).

As ephrin-A ligands can trigger cell retraction and inhibit cell migration, we investigated whether they are sufficient to induce CIL. To test this, Protein A-coated silica beads bound with ephrin-A5–Fc or control Fc were added to cultures of PC-3 cells. Migrating PC-3 cells were contact inhibited by collision with ephrin-A5 beads, but not with control beads (Fig. 2d, e and Supplementary Information, Movies S5 and S6). These data suggest that EphA signalling is a key pathway regulating CIL. Beads coated with either EphA4–Fc or ephrin-B2–Fc did not induce CIL, suggesting that reverse signalling through ephrin-A ligands, or activation of EphB signalling by ephrin-B2, cannot trigger CIL in PC-3 cells (Fig. 2e).

EphA2 and EphA4 mediate homotypic CIL between PC-3 cells

As ephrin-A5–Fc beads were sufficient to induce CIL of PC-3 cells, we predicted that disruption of EphA signalling would prevent homotypic CIL. Reverse transcription–PCR (RT–PCR) analysis revealed that prostate cells predominantly express *EPHA2* and *EPHA4*, and we also detected RT–PCR products for ephrin-A1, ephrin-A3, ephrin-A4 and ephrin-A5 (Supplementary Information, Fig. S3), which are all ligands for these receptors. siRNA oligonucleotides were used to knockdown the expression of EphA2 and EphA4 in PC-3 cells (Fig. 3a), which abolished the binding of ephrin-A ligands (Fig. 3b). Cell retraction was also impaired in these cells when treated with ephrin-A (Fig. 3c, d), confirming that EphA signalling was impaired in the EphA2/EphA4-knockdown cells. Furthermore, on contact, EphA2/EphA4-knockdown cells had defective CIL and maintained forward migration after collision (Fig. 3e–g and Supplementary Information, Movies S7 and S8). We conclude that EphA signalling is necessary for homotypic CIL between PC-3 cells.

Ephrin-B2 induces migration and activates Cdc42 in PC-3 cells

As the migration of PC-3 cells is inhibited by ephrin-A ligands, but enhanced by ephrin-B2 (Fig. 2c), we investigated which ephrin ligands are expressed by the fibroblasts and endothelial cells that PC-3 cells are attracted to. We found that ephrin-A1, ephrin-A3, ephrin-A4 and ephrin-A5 were expressed by fibroblasts and endothelial cells, but all at lower levels than PC-3 cells (Fig. 4a). Interestingly, ephrin-B2 expression is higher in fibroblasts and endothelial cells, compared with PC-3 cells (Fig. 4b). We therefore examined the effects of all the ephrin-B ligands on the migration of prostate cells and found that only ephrin-B2–Fc promoted migration of PC-3 cells in transwell assays (Fig. 4c). Thus, ephrin-B2 can stimulate migration specifically in PC-3 cells, but not in DU-145 cells, and the defective CIL demonstrated by PC-3 cells on contact with fibroblasts and endothelial cells may be because of ephrin-B2 expression by these cells.

Time-lapse microscopy imaging of PC-3 cells following addition of ephrin-B2–Fc revealed a marked increase in membrane ruffling and the formation of multiple leading edges after 20 min (Supplementary Information, Movie S9). We also observed a doubling in the number of fascin-containing filopodia, compared with controls (Fig. 5a, b). Significantly, filopodia induction and transwell migration of PC-3 cells

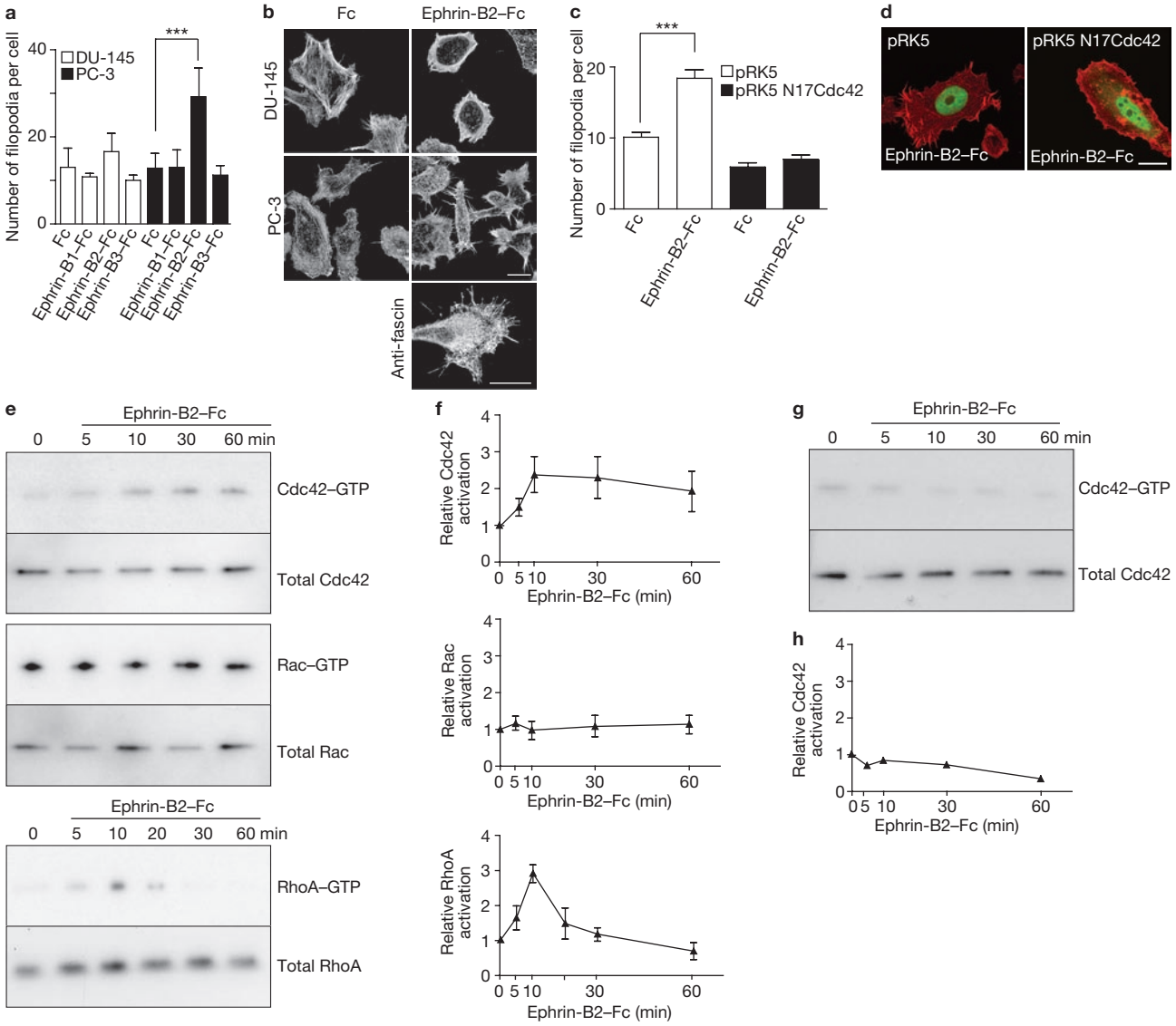

Figure 5 Ephrin-B2 induces filopodia by activating Cdc42 in PC-3 cells. (**a**) DU-145 or PC-3 cells were treated with clustered ephrin-B–Fc or Fc and analysed for the formation of filopodia. Data are expressed as mean number of filopodia per cell ± s.d. ($n = 3$, 50 cells counted per experiment). Triple asterisks indicate $P < 0.001$, as determined by an unpaired Students *t*-test. (**b**) Confocal microscopy images of DU-145 and PC-3 cells treated with clustered ephrin-B2–Fc or Fc and fixed and stained with phalloidin or with antibodies against fascin (PC-3 cell, bottom). (**c**) PC-3 cells were microinjected with expression vectors as indicated, and then treated with ephrin-B2–Fc or Fc, and analysed for the formation of filopodia. Data are expressed as mean number of filopodia per cell ± s.d. (pRK5 and Fc, $n = 92$, pRK5 and ephrin-B2–Fc, $n = 82$; N17Cdc42 and Fc, $n = 87$; N17Cdc42 and ephrin-B2–Fc, $n = 101$). Triple asterisks indicate $P < 0.001$, as determined by an unpaired Student's *t*-test. (**d**) Confocal microscopy images of phalloidin-stained (red) PC-3 cells after microinjection of indicated expression constructs, followed by treatment with ephrin-B2–Fc; injection marker (green). (**e**) PC-3 cells were treated with ephrin-B2–Fc. At the indicated times, cells were lysed, followed by pulldown of Cdc42–GTP, Rac–GTP (using PAK1-CRIB beads) and RhoA–GTP (using Rhotekin Rho-binding domain beads). Proteins were resolved by SDS–PAGE and detected by immunoblotting. (**f**) Quantification of Rho-GTPase activation in PC-3 cells following the addition of ephrin-B2–Fc. Experiments were carried out as in **e**, band intensities were quantified, and normalised intensities were calculated relative to control untreated cells at 0 min. Data are means ± s.d. ($n = 3$). (**g**) DU-145 cells were treated with ephrin-B2–Fc. At the indicated times, cells were lysed, followed by pulldown of Cdc42–GTP using PAK1-CRIB beads. Proteins were resolved by SDS–PAGE and detected by immunoblotting. (**h**) Quantification of Cdc42 activation in DU-145 cells following the addition of ephrin-B2–Fc. Experiments were carried out as in **g**, band intensities were quantified, and normalized intensities were calculated relative to control untreated cells at 0 min. Data are means ($n = 2$). Scale bars: **b**, **d**, 20 μm. Uncropped images of blots are shown in Supplementary Information, Fig. S8.

were specific to ephrin-B2–Fc treatment, and were not observed in DU-145 cells (Fig. 5a, b), suggesting that PC-3 cells express higher levels of EphB receptors than DU-145 cells. Consistent with this hypothesis, and with previous studies[23–25], we found higher levels of EphB2, EphB3 and EphB4 mRNA and protein in PC-3 cells, compared with DU-145 cells (Fig. 4d and Supplementary Information, Fig. S3), explaining why only PC-3 cells show detectable surface binding of ephrin-B2 (Fig. 2a).

Increased migration, coupled with the induction of filopodia, suggested that Cdc42 was being activated downstream of the ephrin-B2 cue. Indeed, injection of PC-3 cells with a dominant-negative Cdc42 expression construct blocked induction of filopodia following the addi-

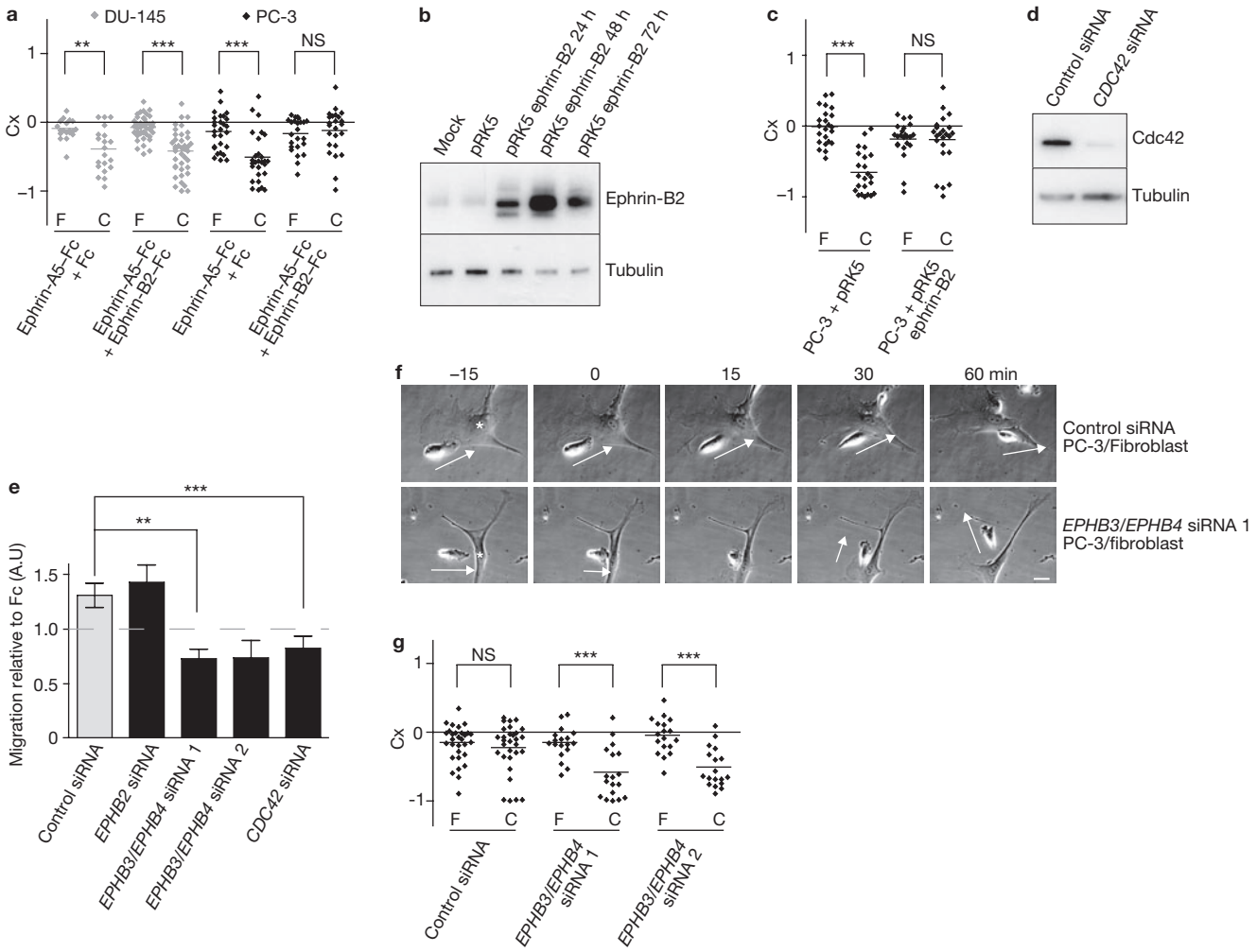

Figure 6 EphB3 and EphB4 knockdown restores CIL of PC-3 cells on contact with fibroblasts. (**a**) Contact acceleration indices (Cx) of free-moving cells (F) versus cells colliding (C) with beads coated with the indicated ephrin–Fc (1:1 molar ratios). DU-145 ephrin-A5–Fc + Fc ($n = 20$), DU-145 ephrin-A5–Fc + ephrin-B2–Fc ($n = 40$), PC-3 ephrin-A5–Fc + Fc ($n = 28$), PC-3 ephrin-A5–Fc + ephrin-B2–Fc ($n = 24$). Triple asterisks indicate $P < 0.001$, double asterisks indicate $P < 0.01$, NS; not significant, as determined by a Mann-Whitney test. (**b**) Immunoblot of lysates from PC-3 cells transfected with no vector (mock), pRK5 or pRK5 containing ephrin-B2 (at the indicated times after transfection), as indicated. Tubulin was used as a loading control.(**c**) Contact acceleration indices (Cx) of free-moving cells (F) versus collisions (C) between PC-3 cells transfected with the indicated plasmids. Cells were imaged between 48–72 h post-transfection. pRK5-transfected cells, $n = 23$, pRK5-ephrin-B2-transfected cells, $n = 23$. Triple asterisks indicate $P < 0.001$, NS; not significant, as determined by a Mann-Whitney test. (**d**) Lysates of PC-3 cells transfected with either control or *CDC42* siRNA oligonucleotides were immunoblotted with antibodies against Cdc42. Tubulin was used as a loading control. (**e**) PC-3 cells transfected with the indicated siRNA oligonucleotides were added to transwell chambers coated with ephrin-B2–Fc, and numbers of cells migrating through were scored. Data are expressed as fold change with respect to control Fc-coated chambers (grey dotted line). Data are means ± s.d. ($n = 5$). Triple asterisks indicate $P < 0.001$, double asterisks indicate $P < 0.01$, as determined by an unpaired Student's *t*-test. (**f**) Representative time-lapse microscopy images, at the indicated times, of a PC-3 cell transfected with control siRNA colliding with a fibroblast (top and Supplementary Information, Movie S10), and a PC-3 cell transfected with *EPHB3* and *EPHB4* siRNA oligonucleotides colliding with a fibroblast (bottom panel and Supplementary Information, Movie S11). White asterisk indicates the fibroblast, arrows indicate direction of migration. Scale bar, 50 μm. (**g**) Contact acceleration indices (Cx) of free-moving cells (F) versus collisions between PC-3 cells and fibroblasts (C). Cells are transfected with the indicated siRNA oligonucleotides. Control ($n = 30$), siRNA 1 ($n = 18$), siRNA 2 ($n = 18$). Triple asterisks indicate $P < 0.001$, NS; not significant, as determined by a Mann-Whitney test. Uncropped images of blots are shown in Supplementary Information, Fig. S8.

tion of ephrin-B2–Fc (Fig. 5c, d) and pulldown studies revealed a sustained activation of Cdc42 in PC-3 cells along with transient activation of RhoA (Fig. 5e, f). No Cdc42 activation was observed in DU-145 cells following addition of ephrin-B2–Fc (Fig. 5g, h).

EphB3/EphB4 knockdown restores CIL when PC-3 cells contact fibroblasts

Ephrin-B2-triggered activation of Cdc42 in PC-3 cells led us to hypothesise that during collision with ephrin-B2-expressing fibroblasts migration may be maintained by locally active Cdc42, which would compete with migration-inhibiting EphA signalling at the site of cell–cell contact.

To test this, we examined collisions of DU-145 and PC-3 cells with beads coated with ephrin-A5–Fc and ephrin-B2–Fc. As expected, ephrin-A5- and ephrin-B2-coated beads did not induce CIL responses in PC-3 cells, but did in DU-145 cells (Fig. 6a). To control against differences in sensitivity between DU-145 and PC-3 cells towards ephrin-A5–Fc,

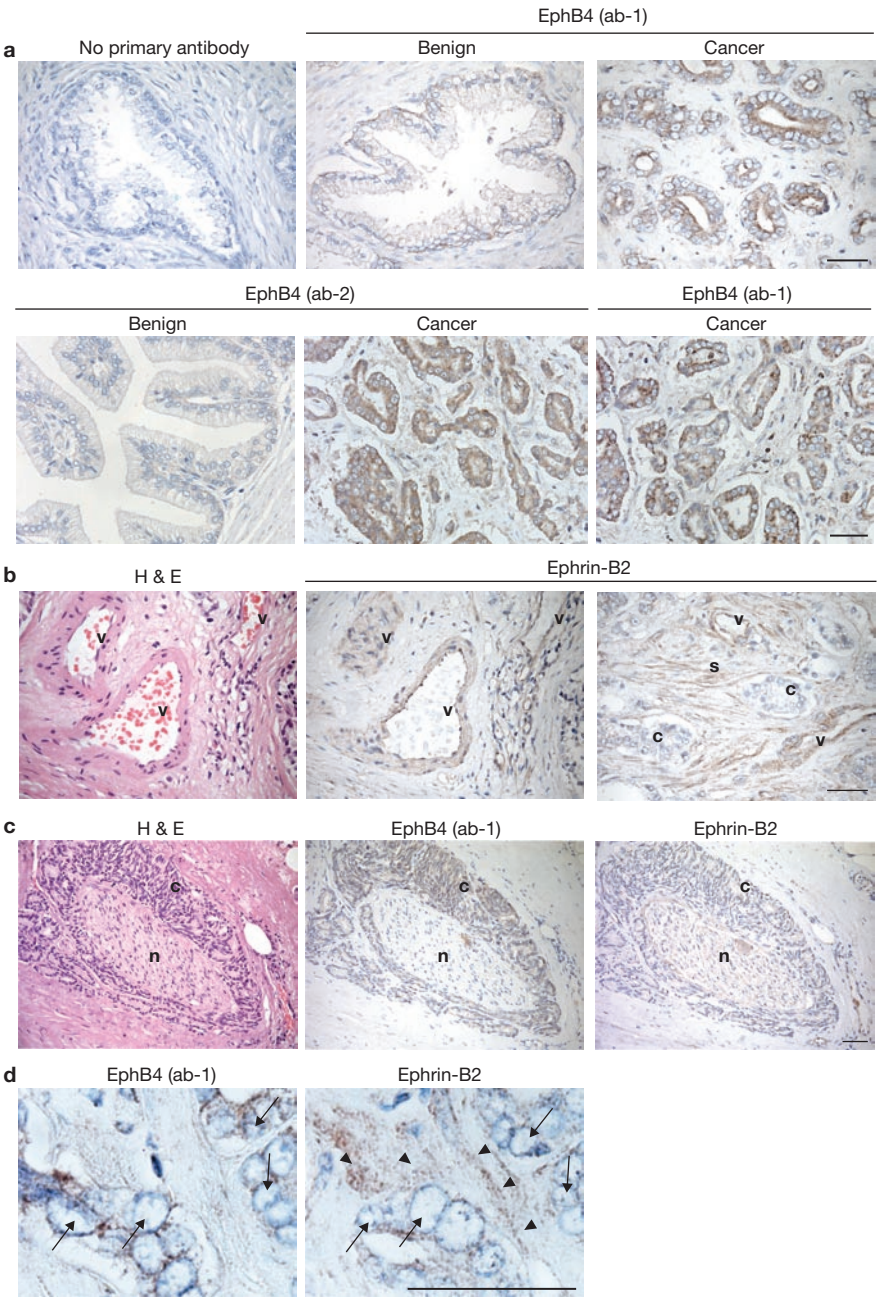

Figure 7 Immunohistochemical staining of EphB4 and ephrin-B2 in prostate cancer. (**a**) EphB4 expression in either benign prostate epithelium or in areas of prostate cancer (Gleason pattern 3+). Top and bottom panels represent sections from two different patients. ab-1 indicates staining with an antibody specific to the EphB4 C-terminal sequence and ab-2 indicates staining with an antibody specific to the EphB4 N-terminal sequence. The increased EphB4 staining was observed in 11 out of 15 cases. (**b**) Ephrin-B2 staining of stromal cells: smooth muscle cells of blood vessels (v) and smooth muscle within the stroma (s). A cohort of cancer cells (c) is indicated. H and E; haematoxylin and eosin. (**c**) An example of perineural invasion showing complementary staining of EphB4 in cancer cells (c) surrounding a nerve fibre (n), and ephrin-B2 in cells within the nerve fibre. (**d**) Complementary staining of EphB4 in cancer cells (nuclei indicated by arrows) and ephrin-B2 staining in the surrounding stromal cells (arrowheads) from serial sections. Similar complementary staining was observed in 6 out of 6 cases. Scale bar, 50 μm.

we coated beads with ephrin-A5–Fc and Fc and found that DU-145 and PC-3 cells demonstrated normal CIL responses to these control beads (Fig. 6a). From these experiments, we conclude that ephrin-B2 competes with the CIL responses induced by ephrin-A5 in PC-3 cells, but not with those in DU-145 cells. In support of the hypothesis that ephrin-B2 competes with ephrin-A-mediated CIL, PC-3 cells overexpressing ephrin-B2 fail to undergo homotypic CIL (Fig. 6b, c).

PC-3 cells express four EphB receptors: EphB2, EphB3, EphB4 and EphB6 (Fig. 4d and Supplementary Information, Fig. S3). Double knockdown of EphB3 and EphB4 abolished the induction of filopodia on treatment of the cells with ephrin-B2–Fc (Supplementary Information, Fig. S4). Additionally, knockdown of EphB3 and EphB4, or Cdc42, decreased PC-3 cell migration through ephrin-B2–Fc coated transwells (Fig. 6d, e), whereas knockdown of EphB2 had no effect. Interestingly,

migration of EphB2-knockdown PC-3 cells is not inhibited by ephrin-B1 ligand in transwell migration assays (Supplementary Information, Fig. S4). The different effects of ephrin-B1 and ephrin-B2 on PC-3 cell migration suggest that EphB receptors might be differentially activated by these two ligands. Indeed, ephrin-B1–Fc markedly activates EphB2 and EphB3, and ephrin-B2–Fc markedly activates EphB4 and EphB3 (Supplementary Information, Fig. S5). These data suggest that EphB3 and EphB4 receptors are required for Cdc42-directed migration toward ephrin-B2 ligand, and EphB2 mediates repulsion triggered by ephrin-B1.

Next, we examined collisions of EphB3/EphB4-knockdown PC-3 cells with fibroblasts and found that most PC-3 cells now demonstrated CIL (Fig. 6f, g and Supplementary Information, Movies S10 and S11). We conclude from these data that upregulation of EphB3 and EphB4 in PC-3 cells prevents them from being contact inhibited by ephrin-B2-expressing fibroblasts, which in turn enables them to invade the substrate territory of this stromal cell. Interestingly, these effects may not be specific to prostate cancer; two breast cancer cell lines expressing EphB3 and EphB4 also indicate defective CIL to fibroblasts, whereas the A549 lung adenocarcinoma cells, that have comparatively low levels of EphB3/B4, are repelled by fibroblasts (Supplementary Information, Fig. S6). However, EphB4 is not sufficient to disrupt CIL because expression of EphB4 in DU-145 cells was not able to perturb repulsion of these cells to fibroblasts (Supplementary Information, Fig. S7).

Complementary expression of EphB4 in prostate cancer cells and ephrin-B2 in neighbouring cells of the tumour microenvironment

To determine whether this signature of EphB and ephrin-B2 that we observe *in vitro* is reflected in prostate cancer *in vivo*, we examined the expression pattern of EphB4 and ephrin-B2 by immunostaining sections of benign or prostate cancer tissue from patients after radical prostatectomy. Staining with two different anti-EphB4 antibodies revealed higher EphB4 expression in prostate cancer (Gleason pattern 3-4), compared with benign prostate epithelium (Fig. 7a), consistent with previous studies[25,26]. Importantly, we found complementary ephrin-B2 expression in several cell types within the adjacent stroma, including smooth muscle cells and endothelial cells of vessels and also cells of nerve fibres, all of which are in contact with the cancer cells (Fig. 7b–d). These data suggest that EphB signalling could potentially be activated in prostate cancer cells by their interactions with ephrin-B2-expressing cells within the neighbouring stroma. These interactions might overcome normal repulsion responses between cells, which restrict cell movements, and thus facilitate cancer-cell invasion.

DISCUSSION

There has been considerable historical interest in the process of CIL following *in vitro* studies that show cancer cells failing to stop migration on contact with non-malignant cells. These observations, from more than thirty years ago, seeded the hypothesis that defective CIL in cancer cells might facilitate the metastatic process[4,5]. However, this hypothesis has never been tested because the molecular cues and signalling pathways underlying CIL have remained elusive.

In this study, we present data that demonstrate a role for EphA–RhoA signalling in repulsive homotypic CIL between prostate cancer cells. Importantly, we find that a failure of CIL by metastatic PC-3 cells in collision with fibroblasts or endothelial cells is because of their elevated levels of EphB3 and EphB4. These receptors are necessary for Cdc42-dependent

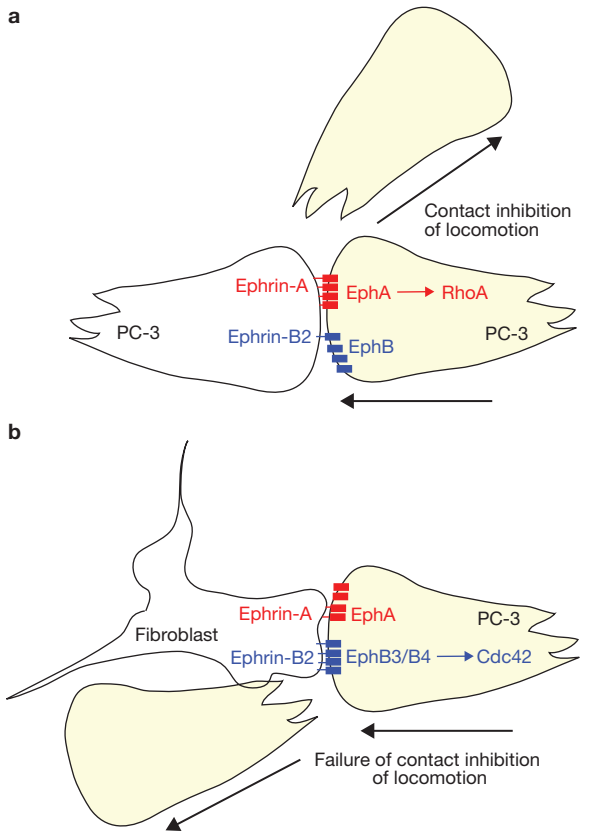

Figure 8 Model of CIL regulation in PC-3 cells. There are two competing pathways that regulate CIL in PC-3 cells; repulsive EphA–RhoA signalling triggered by ephrin-A ligands and attractive EphB3/EphB4–Cdc42 signalling triggered by ephrin-B2 ligand. Thus, the ratio of ephrin-A/ephrin-B2 on a cell will dictate whether the PC-3 cell colliding with it will display CIL or not. (**a**) PC-3 cells have a high ephrin-A/ephrin-B2 ratio and therefore CIL is induced between PC-3 cells by EphA forward signalling, possibly by activation of RhoA. (**b**) Fibroblasts have a high ephrin-B2/ephrin-A ratio which activates EphB3/EphB4–Cdc42 signalling in PC-3 cells, stimulates migration and causes defective CIL.

actin polymerisation and migration towards ephrin-B2 ligand that we show is expressed on fibroblasts and endothelial cells. Furthermore, we demonstrate that knockdown of these two Eph receptors can restore CIL between PC-3 cells and fibroblasts. Thus, the integrated response to repulsive EphA versus attractive EphB3/EphB4 pathways dictates whether the PC-3 cell is repelled or not. Critically, these pathways are activated to different extents depending on the complement of ephrin ligands expressed by the opposing cell in collision (Fig. 8).

We propose that during homotypic CIL between migrating PC-3 cells, engagement of ephrin-A ligands with EphA2 and EphA4 receptors leads to the activation of RhoA at the cell–cell contact site. This halts forward migration in the direction of the collision, the leading lamella is lost and cells repolarise by extending a new leading edge and change their direction of migration. This loss of forward migration may be driven through Rho-regulated actomyosin contraction, triggering membrane withdrawal at the front, coupled with the concurrent inhibition of Rac at the site of cell–cell contact[27,28], or by local Rho–ROCK activity that disrupts cell polarity[29].

In this study, we have analysed the dynamics of individual migrating cells as would be found in high-grade prostate cancer where epithelial

organisation is lost[30]. What role repulsive EphA signalling could have during CIL in cells that have not undergone an epithelial–mesenchymal transition (EMT) and have cell–cell adhesions remains an important question. Interestingly, several studies have implicated cell-adhesion molecules, such as cadherins and nectins in the CIL response[31–33]. It is unlikely that EphA signalling is sufficient for loss of epithelial organisation in prostate cancer because these cancer cell lines, expressing EphA and ephrinA ligands, require HGF to undergo an EMT.

Although activation of RhoA can lead to loss of lamellipodia, activation of Rac and Cdc42 can regulate attraction responses by locally stimulating actin polymerization and by maintaining the direction of polarised migration through microtubule capture at the cell's leading edge[34]. Here, we demonstrate that ephrin-B2, which is expressed in fibroblasts and endothelial cells, can trigger sustained activation of Cdc42, filopodia extension and increased migration in isolated PC-3 cells. This response is comparable to the activation of Cdc42 and Rac by EphB receptors in the synapse that leads to the formation of new dendritic spines[35,36]. Previously, we showed that ephrin-B2 mediates cell repulsion through EphB4 in fibroblasts and endothelial cells[37]. Further work is required to understand the paradox of the ephrin-B2 response. It is worth noting that in a previous study[37] initial ephrin-B2–EphB4 interactions stimulated lamellipodia and filopodia production coupled with forward protrusion in EphB4-expressing cells and that, only after sustained interaction, was the subsequent internalisation of EphB4 and cell repulsion observed. However, we cannot exclude that the HGF treatment used to stimulate migration in this study may affect signalling events in response to Eph receptors.

Our studies indicate that elevated levels of EphB3 and EphB4 by prostate cancer cells could promote local invasion because cancer cells would be released from normal CIL restraints provided by surrounding non-cancer cells expressing ephrin-B2. Although little is known about the role of EphB3 in prostate cancer, other studies have shown that EphB4 is required for prostate tumour growth *in vivo*[25]. EphB4 has been shown to have both pro- and anti-tumour properties in breast and colon cancer, but it is generally associated with a more invasive phenotype[38]. In contrast, EphB2, which we show not to be required for defective CIL in PC-3 cells, is thought to function as a tumour suppressor in prostate and colon cancer[24,39] and to restrict cell intermingling through repulsion triggered by ephrin-B1[40]. Here, we show that EphB2/EphB3 are preferentially activated by ephrin-B1 in PC-3 cells, and that the EphB2–ephrin-B1 interaction inhibits PC-3 cell migration. This is in contrast with the effects of ephrin-B2 that we show preferentially activates EphB4/EphB3 and stimulates cell migration. These data suggest that EphB2 and EphB4 mediate opposite effects on prostate cell interactions and are consistent with their roles in colon cancer[41].

Importantly, our immunohistochemistry studies confirm previous reports that levels of EphB4 are elevated in advanced human prostate cancer[25,26] and also demonstrate a complementary expression of ephrin-B2 by various stromal cell types. These cells will be in direct contact with cohorts of invasive prostate cancer cells (Gleason pattern 4-5) because they lack a basement membrane[30]. These data illustrate the relevance of our *in vitro* studies and indicate that within a tumour ephrin-B2 is expressed spatially precisely where it can activate EphB3 and EphB4 on cancer cells. We propose that upregulation of EphB3 and EphB4 in prostate cancer could aid the local invasion and possibly the metastatic spread of prostate cancer cells through deregulation of CIL.

METHODS

Methods and any associated references are available in the online version of the paper at http://www.nature.com/naturecellbiology/

Note: Supplementary Information is available on the Nature Cell Biology website

ACKNOWLEDGEMENTS

We thank H. Ross for technical assistance and I. Hers for advice on immunoprecipitations, M. Brown for BMECs, A. Ziemiecki and A. -C. Andres for anti-EphB4, D. Wilkinson for anti-EphA4 and E. Pasquale for anti-EphB3. We thank P. Martin, N. Perkins and C. Paraskeva for critically reading the manuscript. We are grateful to J. Dovovan and NCRI/MRC ProMPT collaborative for facilitating clinical aspects of the work. This study has been approved by the Southmead Research Ethics Committee and was funded by a Wellcome Trust PhD studentship to J.B., an MRC studentship to S.K. and a Cancer Research UK project grant to C.D.N.

AUTHOR CONTRIBUTIONS

J.W.A., S.K. and C.D.N. designed experiments. J.W.A. and J.C. performed the RT–PCR, J.B. performed the Cdc42-knockdown experiments, C.D.N. performed microinjection experiments and immunohistochemistry, and J.W.A. carried out all other experiments. D.G. and R.P. provided prostate tissue and J.O., J.W.A. and C.D.N. prepared and analysed prostate immunohistochemistry. J.W.A. and C.D.N. wrote the manuscript.

COMPETING INTERESTS STATEMENT

The authors declare no competing financial interests.

Published online at http://www.nature.com/naturecellbiology
Reprints and permissions information is available online at http://npg.nature.com/reprintsandpermissions/

1. Abercrombie, M. Contact inhibition in tissue culture. *In Vitro* **6,** 128–142 (1970).
2. Abercrombie, M. & Turner, A. A. Contact reactions influencing cell locomotion of a mouse sarcoma in culture. *Med. Biol.* **56,** 299–303 (1978).
3. Paddock, S. W. & Dunn, G. A. Analysing collisions between fibroblasts and fibrosarcoma cells: fibrosarcoma cells show an active invasionary response. *J. Cell Sci.* **81,** 163–187 (1986).
4. Abercrombie, M. Contact inhibition and malignancy. *Nature* **281,** 259–262 (1979).
5. Vesely, P. & Weiss, R. A. Cell locomotion and contact inhibition of normal and neoplastic rat cells. *Int. J. Cancer* **11,** 64–76 (1973).
6. Gaggioli, C. *et al.* Fibroblast-led collective invasion of carcinoma cells with differing roles for RhoGTPases in leading and following cells. *Nat. Cell Biol.* **9,** 1392–1400 (2007).
7. Wyckoff, J. *et al.* A paracrine loop between tumor cells and macrophages is required for tumor cell migration in mammary tumors. *Cancer Res.* **64,** 7022–7029 (2004).
8. Carmona-Fontaine, C. *et al.* Contact inhibition of locomotion *in vivo* controls neural crest directional migration. *Nature* **456,** 957–961 (2008).
9. Stramer, B. *et al.* Clasp-mediated microtubule bundling regulates persistent motility and contact repulsion in Drosophila macrophages *in vivo*. *J. Cell Biol.* **189,** 681–689 (2010).
10. Kullander, K. & Klein, R. Mechanisms and functions of Eph and ephrin signalling. *Nat. Rev. Mol. Cell Biol.* **3,** 475–486 (2002).
11. Poliakov, A., Cotrina, M. & Wilkinson, D. G. Diverse roles of eph receptors and ephrins in the regulation of cell migration and tissue assembly. *Dev. Cell* **7,** 465–480 (2004).
12. Pasquale, E. B. Eph–ephrin bidirectional signaling in physiology and disease. *Cell* **133,** 38–52 (2008).
13. Pasquale, E. B. Eph receptor signalling casts a wide net on cell behaviour. *Nat. Rev. Mol. Cell Biol.* **6,** 462–475 (2005).
14. Noren, N. K. & Pasquale, E. B. Eph receptor-ephrin bidirectional signals that target Ras and Rho proteins. *Cell Signal* **16,** 655–666 (2004).
15. Merlos-Suarez, A. & Batlle, E. Eph–ephrin signalling in adult tissues and cancer. *Curr. Opin. Cell Biol.* **20,** 194–200 (2008).
16. Surawska, H., Ma, P. C. & Salgia, R. The role of ephrins and Eph receptors in cancer. *Cytokine Growth Factor Rev.* **15,** 419–433 (2004).
17. Mickey, D. D., Stone, K. R., Wunderli, H., Mickey, G. H. & Paulson, D. F. Characterization of a human prostate adenocarcinoma cell line (DU 145) as a monolayer culture and as a solid tumor in athymic mice. *Prog. Clin. Biol. Res.* **37,** 67–84 (1980).
18. Kaighn, M. E., Narayan, K. S., Ohnuki, Y., Lechner, J. F. & Jones, L. W. Establishment and characterization of a human prostatic carcinoma cell line (PC-3). *Invest. Urol.* **17,** 16–23 (1979).
19. Kozlowski, J. M. *et al.* Metastatic behavior of human tumor cell lines grown in the nude mouse. *Cancer Res.* **44,** 3522–3529 (1984).
20. Zhu, A., Zhang, C. X. & Lieberman, H. B. Rad9 has a functional role in human prostate carcinogenesis. *Cancer Res.* **68,** 1267–1274 (2008).
21. Huang, X., Wu, D., Jin, H., Stupack, D. & Wang, J. Y. Induction of cell retraction by the combined actions of Abl–CrkII and Rho–ROCK1 signaling. *J. Cell Biol.* **183,** 711–723 (2008).
22. Parri, M. *et al.* EphrinA1 activates a Src/focal adhesion kinase-mediated motility response leading to rho-dependent actino/myosin contractility. *J. Biol. Chem.* **282,** 19619–19628 (2007).

23. Chaib, H., Cockrell, E. K., Rubin, M. A. & Macoska, J. A. Profiling and verification of gene expression patterns in normal and malignant human prostate tissues by cDNA microarray analysis. *Neoplasia* **3,** 43–52 (2001).
24. Huusko, P. *et al.* Nonsense-mediated decay microarray analysis identifies mutations of EPHB2 in human prostate cancer. *Nat. Genet.* **36,** 979–983 (2004).
25. Xia, G. *et al.* EphB4 expression and biological significance in prostate cancer. *Cancer Res.* **65,** 4623–4632 (2005).
26. Lee, Y. C. *et al.* Investigation of the expression of the EphB4 receptor tyrosine kinase in prostate carcinoma. *BMC Cancer* **5,** 119 (2005).
27. Wegmeyer, H. *et al.* EphA4-dependent axon guidance is mediated by the RacGAP α2-chimaerin. *Neuron* **55,** 756–767 (2007).
28. Iwasato, T. *et al.* Rac–GAP α-chimerin regulates motor-circuit formation as a key mediator of EphrinB3/EphA4 forward signaling. *Cell* **130,** 742–753 (2007).
29. Nakayama, M. *et al.* Rho-kinase phosphorylates PAR-3 and disrupts PAR complex formation. *Dev. Cell* **14,** 205–215 (2008).
30. Bostwick, D. G., Leske, D. A., Qian, J. & Sinha, A. A. Prostatic intraepithelial neoplasia and well differentiated adenocarcinoma maintain an intact basement membrane. *Pathol. Res. Pract.* **191,** 850–855 (1995).
31. Bracke, M. E. *et al.* Functional downregulation of the E-cadherin–catenin complex leads to loss of contact inhibition of motility and of mitochondrial activity, but not of growth in confluent epithelial cell cultures. *Eur. J. Cell Biol.* **74,** 342–349 (1997).
32. Huttenlocher, A. *et al.* Integrin and cadherin synergy regulates contact inhibition of migration and motile activity. *J. Cell Biol.* **141,** 515–526 (1998).
33. Takai, Y., Miyoshi, J., Ikeda, W. & Ogita, H. Nectins and nectin-like molecules: roles in contact inhibition of cell movement and proliferation. *Nat. Rev. Mol. Cell Biol.* **9,** 603–615 (2008).
34. Etienne-Manneville, S. Cdc42—the centre of polarity. *J. Cell Sci.* **117,** 1291–1300 (2004).
35. Irie, F. & Yamaguchi, Y. EphB receptors regulate dendritic spine development via intersectin, Cdc42 and N-WASP. *Nat. Neurosci.* **5,** 1117–1118 (2002).
36. Penzes, P. *et al.* Rapid induction of dendritic spine morphogenesis by trans-synaptic ephrinB–EphB receptor activation of the Rho-GEF kalirin. *Neuron* **37,** 263–274 (2003).
37. Marston, D. J., Dickinson, S. & Nobes, C. D. Rac-dependent trans-endocytosis of ephrinBs regulates Eph–ephrin contact repulsion. *Nat. Cell Biol.* **5,** 879–888 (2003).
38. Noren, N. K. & Pasquale, E. B. Paradoxes of the EphB4 receptor in cancer. *Cancer Res.* **67,** 3994–3997 (2007).
39. Genander, M. *et al.* Dissociation of EphB2 signaling pathways mediating progenitor cell proliferation and tumor suppression. *Cell* **139,** 679–692 (2009).
40. Cortina, C. *et al.* EphB–ephrin-B interactions suppress colorectal cancer progression by compartmentalizing tumor cells. *Nat. Genet.* **39,** 1376–1383 (2007).
41. Kumar, S. R. *et al.* Preferential induction of EphB4 over EphB2 and its implication in colorectal cancer progression. *Cancer Res.* **69,** 3736–3745 (2009).

DOI: 10.1038/ncb2122

METHODS

Cell culture and reagents. DU-145, PC-3, MCF-7 and MDA-MB-231 cells were obtained from the ECACC, BMECs were a gift from M. Brown, (University of Manchester, UK) and A549 cells were a gift from J. Tavaré (University of Bristol, UK). PrEC and nHDF cells were obtained from Lonza. The epithelial origin of the three prostate cell lines was confirmed by positive pan-cytokeratin staining (data not shown).

DU-145, PC-3, MCF-7, MDA-MB-231 and A549 cells were maintained in RPMI-1640 media (Sigma) supplemented with 10% (v/v) FBS (fetal bovine serum; PAA), 2 mM L-glutamine, 100 units ml^{-1} penicillin and 0.1 mg ml^{-1} streptomycin. PrEC cells were maintained in supplemented prostate epithelial cell growth media (Lonza). Cells were grown at 37 °C with 5% CO_2. PrEC and nHDF cells were maintained for only three passages and at least two independent batches of each cell type were used in this study.

Ephrin–Fc and Eph–Fc proteins, and HGF, were obtained from R&D systems. Blebbistatin was from Tocris, and Y27632 was from Calbiochem. pRK5-ephrin-B2 and pRK5-EphB4 were as described previously[37,42].

The following antibodies were used in this study: anti-ephrin-B2 (rabbit polyclonal, Sigma), anti-EphB2 (goat polyclonal, R&D systems), anti-EphA2 (mouse monoclonal, Upstate), anti-EphB4 (N-terminal, rabbit polyclonal H-200, Santa Cruz)[43], anti-α-tubulin (mouse monoclonal, Serotec), anti-RhoA (mouse monoclonal, Cytoskeleton), anti-Rac (mouse monoclonal, Upstate), anti-Cdc42 (mouse monoclonal, Transduction Laboratories), anti-Fascin (mouse monoclonal SSK2, DAKO) and anti-phosphotyrosine clone 4G10 (mouse monoclonal, Millipore). Rabbit polyclonal anti-EphA4 was a gift from D. Wilkinson (NIMR, UK), rabbit polyclonal anti-EphB4 (C-terminal) was a gift from A. -C. Andres (University of Bern, Germany)[44] and rabbit polyclonal anti-EphB3 was a gift from E. Pasquale (Burnham Institute, USA). Antibody dilutions are detailed in Supplementary Information, Table 1.

Statistics. As Cx values are not normally distributed (determined by a normal quantile plot of the Cx values) the non-parametric Mann-Whitney U-test was used to determine significance. In all other cases a two-tailed Student's *t*-test was used.

Time-lapse imaging and confocal microscopy. Time-lapse microscopy imaging was performed on an inverted Zeiss microscope with an Orca-ER camera (Hamamatsu) and Improvision software. An image was taken every 15 s at 37 °C with 5% CO_2 for up to 10 h. Otherwise, to record large numbers of cell–cell collisions, phase-contrast time-lapse microscopy was performed on an inverted Leica DMIRE microscope equipped with a Maerzhaeuser scanning stage for multi-position imaging, at 37 °C, and cells were maintained in CO_2-independent media (Invitrogen). An image was taken every 5 min using a ×10 objective. Image analysis was performed using Volocity software (Improvision).

Confocal microscopy of fixed cells was performed on a Leica SP5 confocal microscope. Cell staining was performed as previously described[37]. In some cases, filopodia were preserved by adding glutaraldehyde (1% v/v) to the fix buffer. For fascin staining, cells were fixed in −20 °C methanol. In Figure 2b, prostate cells were treated with clustered ephrin–Fc proteins for 10 min before fixation and phalloidin staining. In Figure 3c, d, PC-3 cells, transfected with siRNA oligonucleotides as indicated, were treated with clustered ephrin-A1–Fc, ephrin-A5–Fc or Fc for 10 min, and rounded cells were counted after fixation (10 min) and staining with 0.1 μg ml^{-1} phalloidin (Molecular Probes). In Figure 5b, c DU-145 or PC-3 cells were treated with clustered ephrin-B2–Fc or Fc for 20 min.

Contact inhibition of locomotion. For analysis of homotypic collisions, 3,000–4,000 cells were grown on 13 mm glass coverslips coated with matrigel (diluted 1 in 3 with culture medium; Sigma) for 24 h. PC-3 and DU-145 cells were serum starved (RPMI supplemented with 0.5% (v/v) FCS) for 24 h before addition of HGF (10 ng ml^{-1}) for a further 16 h to stimulate cell migration. PrEC cells were grown for 24 h in basal PrEGM media for 24 h, before addition of HGF. For heterotypic collisions, prostate cells were co-cultured with nHDF or BMEC cells, and one cell type was labelled with 2 μM cell tracker green (Molecular Probes) allowing analysis of appropriate collisions.

Quantification of CIL was carried out as described previously[3]. Briefly, the displacement of a migrating cell for 50 min before collision (Fig. 1b, vector A) and for 50 min following collision (vector B) was measured. For PrEC cells, which migrate at twice the speed of DU-145 or PC-3 cells, displacements over 25 min periods were measured. The component Cx of vector B–A represents the difference between how far the cell has progressed in the direction of A' and how far it would have gone had there been no collision. Cx values were also calculated for the same population of cells that were free-moving and not colliding, by tracking cell movements over the same time periods. CIL was considered to have occurred when the mean Cx value of free-moving cells was significantly different to that of colliding cells as determined using a Mann-Whitney U-test. The centre of the nucleus was used as a marker to track vectors A and B. Only head-on collisions of leading edge lamellae were analysed and collisions where a third cell was involved were excluded. Cx measurements were scaled to normalize for differences in speed between cell populations.

Collagen invasion assay. This method was as previously described[45]. Briefly, 24-well 8 μm transwell inserts (BD) were filled with 50 μl of Collagen I (BD), inverted, and coated with 1.5×10^4 serum-starved PrECs, DU-145 or PC-3 cells labelled with 2 μM cell tracker green (Molecular Probes). Transwells were placed in 24-well plates and filled with serum-free media with 10 ng ml^{-1} HGF and cells were left at 37 °C for 48 h to migrate into the collagen. Experiments were done in triplicate. Tranwells were fixed, and fluorescent cells were imaged using a Leica AOBS SP2 inverted confocal microscope (Leica). Optical sections were taken every 5 μm and cells were identified and counted using Volocity software (Improvision).

Transwell migration assay. Transwell inserts (24 wells, 8 μm; BD) were coated on the bottom surface with 2 μg ml^{-1} ephrin–Fcs[46]. Into each transwell, 5×10^4 serum-starved PrECs, DU-145 or PC-3 cells were seeded, fluorescently labelled with 2 μM cell tracker green (Molecular Probes) and treated with 10 ng ml^{-1} HGF. Transwells were left overnight at 37 °C and 5% CO_2 before fixing cells, removing those cells from inner membrane, and counting the cells that had migrated through to the underside. Each experiment was conducted in triplicate and included 2 μg ml^{-1} Fc-coated transwells as a control. The number of migrated cells per transwell was obtained by adding the cells counted in ten fields of view, using a ×20 objective.

Cell stimulation, immunoprecipitation and western blotting. Serum-starved PrEC, DU-145 and PC-3 cells, cultured on 6 cm dishes or matrigel-coated coverslips, were treated with ephrin–Fc chimeras (1 μg ml^{-1}) pre-clustered for 30 min at 37 °C with goat anti-human-Fc antibody (10 μg ml^{-1}, Stratech). For western blotting, cells were serum starved at 50% confluence, and treated with 10 ng ml^{-1} HGF. Cells were washed once in cold PBS before lysing in RIPA buffer for 10 min on ice. Lysates were vortexed for 10 min, centrifuged and the supernatant retained.

The levels of Rho GTPase–GTP were measured using a RhoA–GTP pulldown kit (Cytoskeleton); Cdc42–GTP and Rac–GTP pulldowns were performed using PAK1:CRIB beads (Upstate), according to the manufacturer's instructions. Bands were quantified and normalised intensities expressed relative to 0 min control (assigned as 1).

Eph-receptor activation following ephrin–Fc treatment was determined by immunoprecipitation of Eph receptors with appropriate antibodies followed by incubation with Protein A or Protein G–Sepharose beads (Sigma).

Preparation of ephrin–Fc-coated beads. Protein A-coated 10 μm-diameter silica beads (G. Kisker) were incubated with 1 μg ml^{-1} ephrin–Fc overnight at 4 °C, centrifuged, washed with PBS and then blocked for 1 h in 2% (v/v) BSA (bovine serum albumin)/PBS before resuspension in cell media. For beads coated with both ephrin-B2–Fc and ephrin-A5–Fc, a solution containing 1 μg ml^{-1} of each ephrin–Fc was used (1:1 molar ratio). For beads coated with both ephrin-A5–Fc and Fc a solution containing 1 μg ml^{-1} of ephrin-A5–Fc and 3.23 μg ml^{-1} of Fc was used (1:1 molar ratio).

Real-time RT–PCR. RNA was extracted using the RNAeasy kit (Qiagen) from cells that were serum starved, treated with 10 ng ml^{-1} HGF and 50% confluent. RNA (10 μg) was treated with 2.5 units DNase (Roche). cDNA was synthesised from 1 μg DNase-treated RNA using 0.3 μg random primers (Sigma) and 200 units reverse transcriptase (Promega). Real-time PCR was performed on a 1:10 dilution of cDNA using the Sensimix sybergreen PCR mastermix (Quantace) and an Opticon thermocycler (MJ research). Standard PCR was performed using Hotstar Taq mastermix (Qiagen). Primers for PCR are detailed in the Supplementary Information, Table 1 and the identity of all PCR products obtained was confirmed by DNA sequencing. Human brain RNA (Ambion) was used as a positive control for primers that did not amplify products from cell line RNA.

siRNA. Between 10–25 nM siRNA oligonucleotides (Dharmacon) were transfected into PC-3 cells using Dharmafect 2 reagent (Dharmacon), according to the manufacturer's instructions. Transfected cells were imaged between 72 and 96 h post-transfection. siRNA oligonucleotide sequences are detailed in Supplementary Information, Table 1. Two different siRNAs were used for EphA2, EphA4, EphB3 and EphB4 knockdown. For all siRNA experiments, a non-targeting siRNA oligonucleotide was used as negative control.

Cell microinjection. Cell nuclei were microinjected with pRK5-N17Cdc42 (100 μg ml^{-1}) and an injection marker (Fluorescein isothiocyanate; FITC-conjugated lysinated dextran; Molecular Probes). Cells were allowed 3 h to express recombinant protein before treatment with ephrin-B2–Fc.

Cell transfection. DU-145 and PC-3 cells were transfected with pRK5 expression vectors using the TransIT Prostate Transfection Kit (Mirus Bio), according to the manufacturer's instructions.

Immunohistochemistry. We evaluated tissue sections from formaldehyde-fixed paraffin embedded prostate tissue obtained from 15 different patients with prostate cancer (eleven from J. D. Oxley, Southmead Hospital Bristol, UK; four from a tissue array, AccuMax). Sections were de-waxed in Histoclear (National Diagnostics), hydrated in graded ethanols, quenched for 17 min in 0.6% (v/v) hydrogen peroxide before antigen retrieval by boiling in 10 mM citrate buffer (pH 6). Immunolabelling was undertaken using the VECTASTAIN Elite ABC kit (Vector Labs) according to the manufacturer's instructions. Slides were counterstained in Gills Haemotoxylin (Vector Labs) before mounting in DPX (BDH).

42. Bochenek, M. L., Dickinson, S., Astin, J. W., Adams, R. H. & Nobes, C. D. Ephrin-B2 regulates endothelial cell morphology and motility independently of Eph-receptor binding. *J. Cell. Sci.* **123,** 1235–1246 (2010).
43. Stephenson, S. A., Slomka, S., Douglas, E. L., Hewett, P. J. & Hardingham, J. E. Receptor protein tyrosine kinase EphB4 is up-regulated in colon cancer. *BMC Mol. Biol.* **2,** 15 (2001).
44. Munarini, N. *et al.* Altered mammary epithelial development, pattern formation and involution in transgenic mice expressing the EphB4 receptor tyrosine kinase. *J. Cell Sci.* **115,** 25–37 (2002).
45. Hooper, S., Marshall, J. F. & Sahai, E. Tumor cell migration in three dimensions. *Methods Enzymol.* **406,** 625–643 (2006).
46. Matsuoka, H., Obama, H., Kelly, M. L., Matsui, T. & Nakamoto, M. Biphasic functions of the kinase-defective Ephb6 receptor in cell adhesion and migration. *J. Biol. Chem.* **280,** 29355–29363 (2005).

nature cell biology

DOI: 10.1038/ncb2122

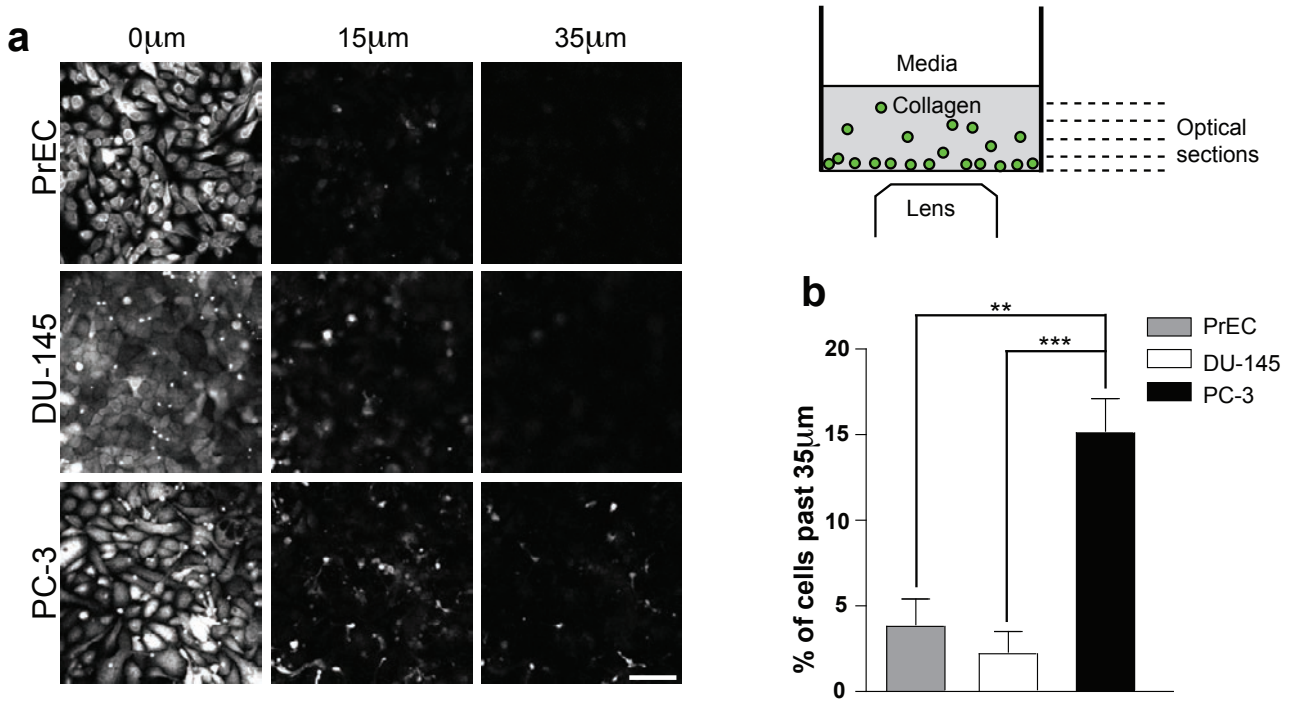

Figure S1 PC-3 cells are invasive *in vitro.* (**a**) Optical confocal Z sections from collagen I invasion assays. PrEC, DU-145 and PC-3 cells were labeled with cell-tracker green and allowed to invade into collagen I for 48 h before fixation and imaging. Example z-sections from 0, 15 and 35 μm showing that PC-3 cells have invaded into the collagen I in the presence of HGF. Scale bar = 150 μm. (**b**) Quantitation of the collagen I invasion showing the percentage of cells that had invaded past 35 μm. Values are means ± s.d. (n=3). *** p<0.001, ** p<0.01 determined by an unpaired students t-test.

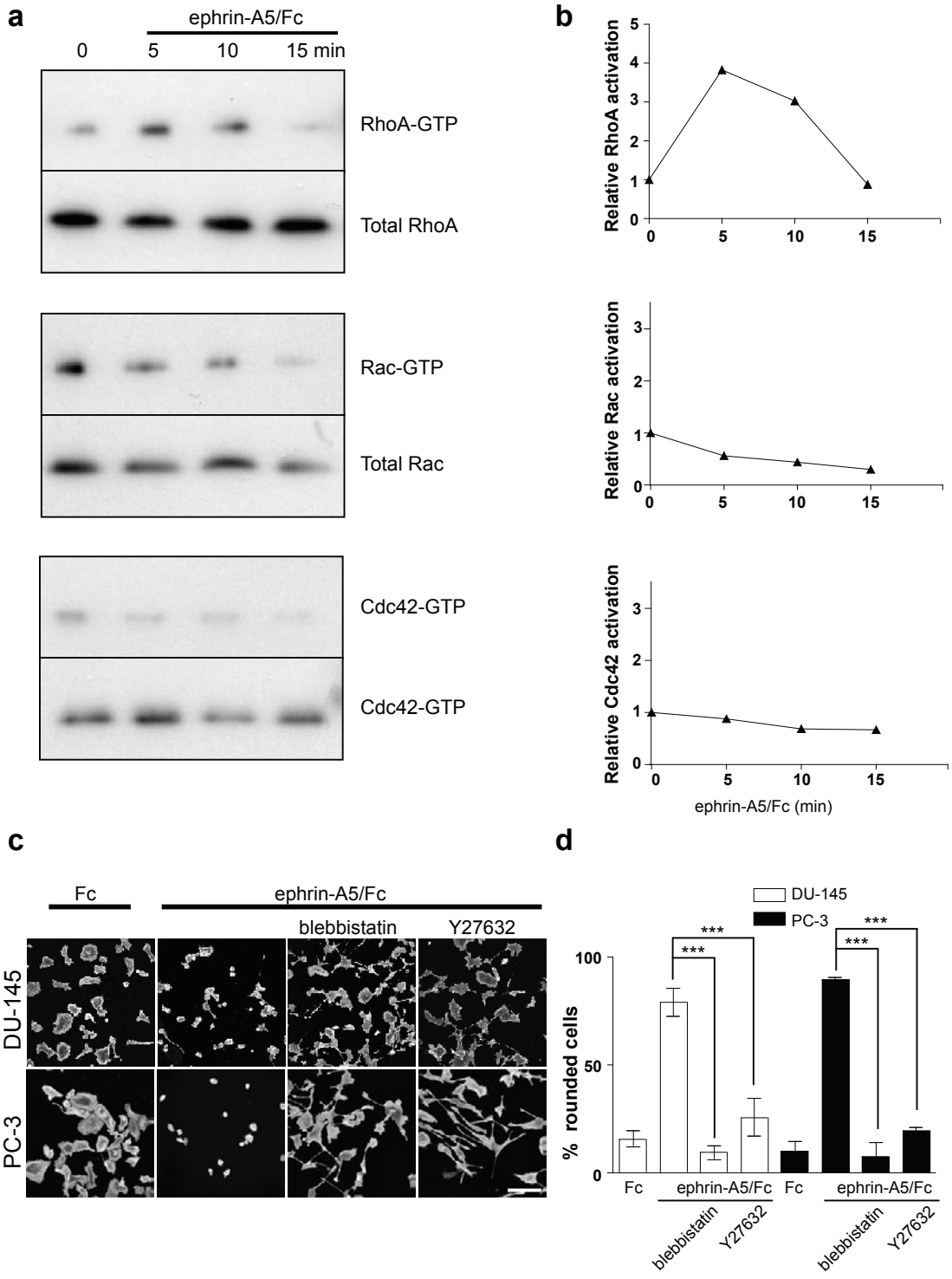

Figure S2 Ephrin-A5 activates RhoA and causes actomyosin dependent cell rounding. (**a**) Lysates of PC-3 cells after pulldowns of RhoA-GTP, using Rhotekin Rho-binding domain beads, Rac-GTP and Cdc42-GTP using PAK1-CRIB beads. (**b**) Quantitation of Rho-GTPase activation in PC-3 cells following the addition of ephrin-A5/Fc. Bands were quantified and normalised intensities were calculated relative to control untreated 0min cells. Values are means (n=2). (**c**) Ephrin-A5/Fc-induced cell rounding is actomyosin dependent. Prostate cells were pretreated for 2 h with the myosin II inhibitor, blebbistatin (50 μM) or with the Rho kinase (ROCK) inhibitor, Y27632 (20 μM) and then clustered ephrin-A5/Fc was added for 10 min before fixation and phalloidin staining. Scale bar = 100 μm. (**d**) Graph shows the percentage of cells that were rounded. Values are means ± s.d. (n=3, 100 cells counted per experiment). *** $p<0.001$, determined by an unpaired students t-test.

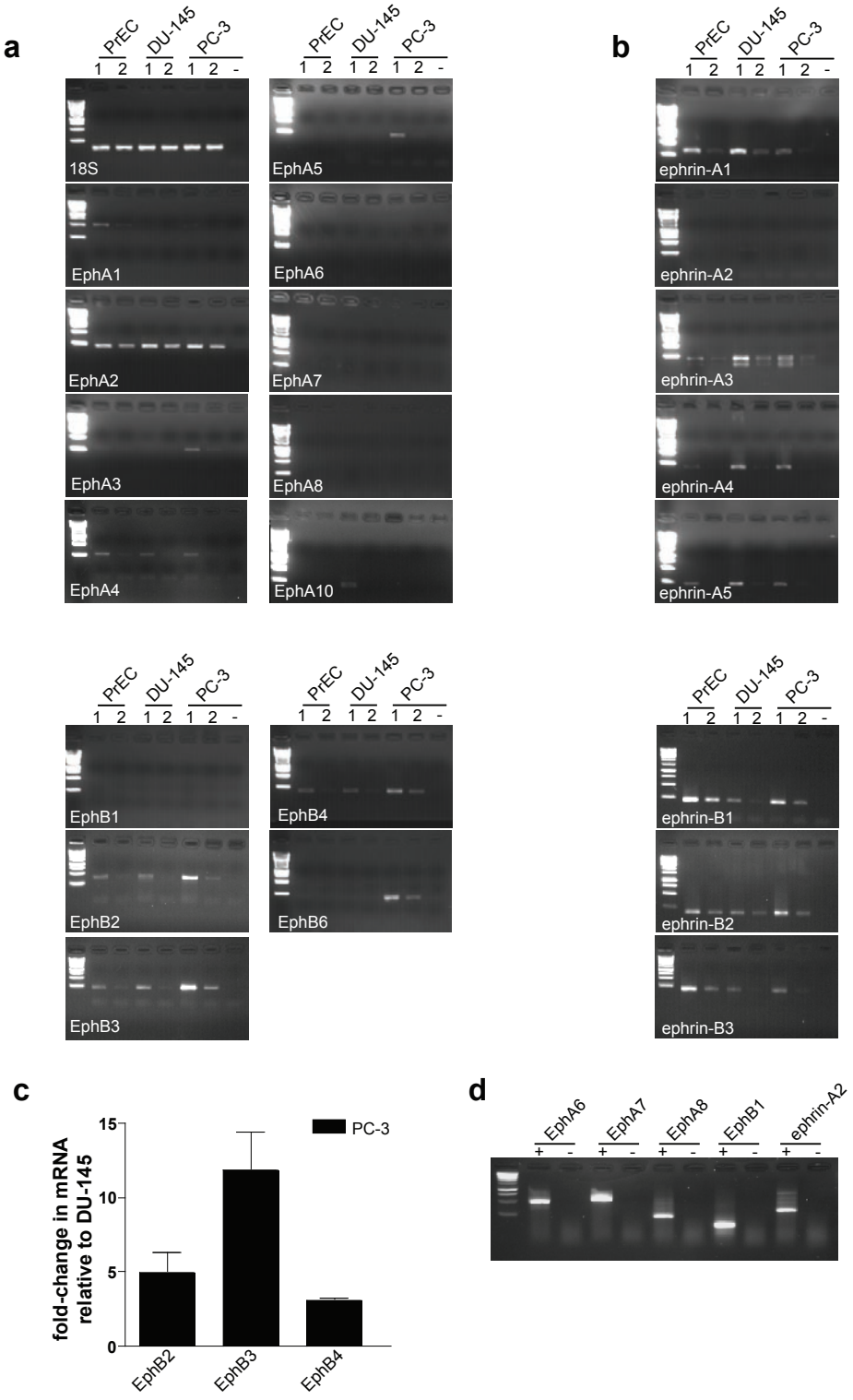

Figure S3 Expression of Eph receptors and ephrin ligands in prostate cell lines. Agarose gels showing RT-PCR products from cDNA diluted either 1/10 (1) or 1/100 (2). A no reverse transcriptase control for PC-3 cells is shown with (-). RT-PCR was performed using primers against either Eph receptors (**a**) or ephrin ligands (**b**). (**c**) Relative expression profiles of EphB2, B3 and B4 in PC-3 versus DU-145 cells as determined by Real-time RT-PCR. Data are expressed as fold change with respect to DU-145 cell mRNA. Values are means ± s.d. (n=3). (**d**) RT-PCR reactions using cDNA created from human brain RNA, either with (+) or without (-) reverse transcriptase were used as a positive control for primers that did not amplify products from cell line RNA.

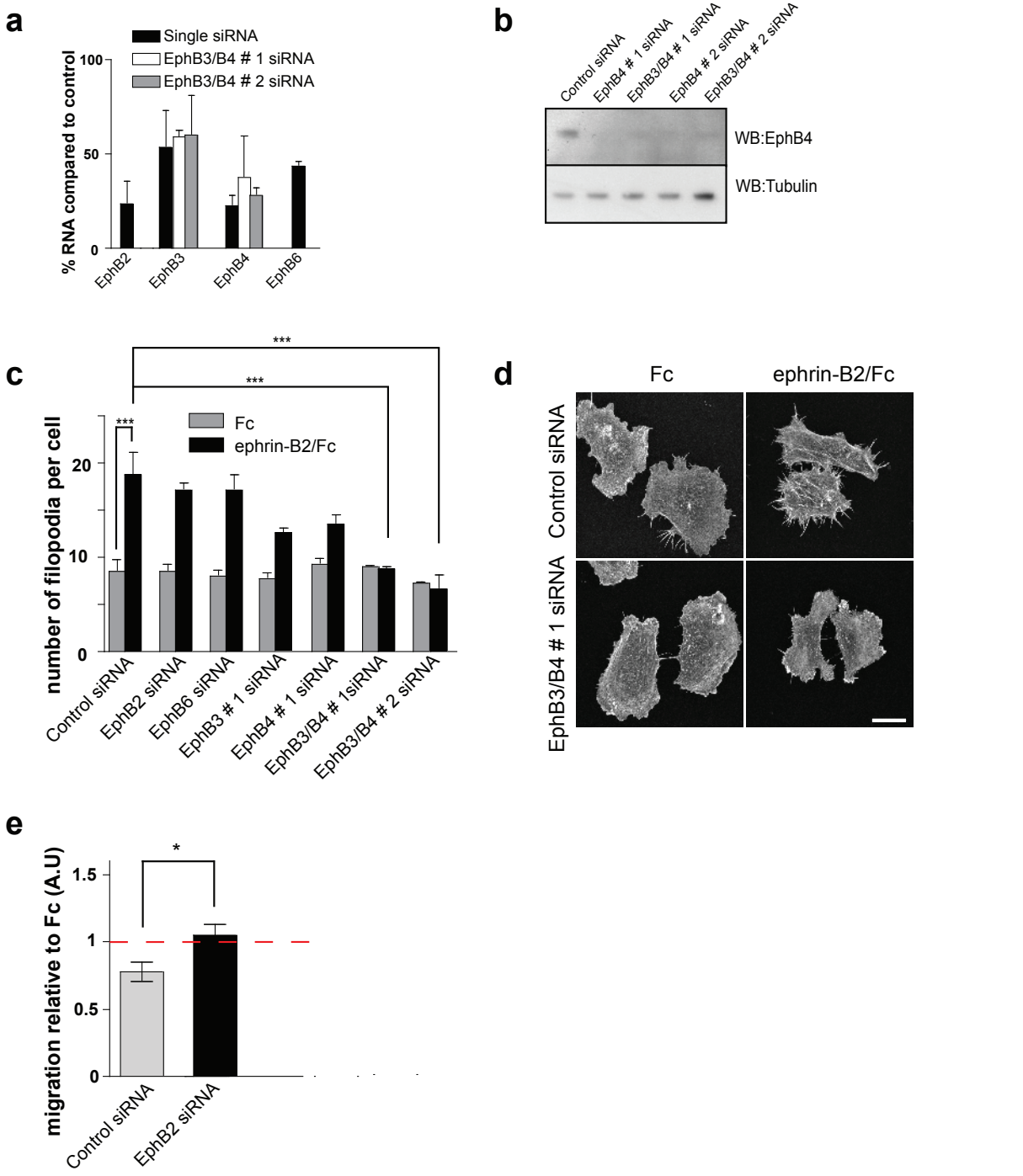

Figure S4 siRNA silencing of EphB receptors in PC-3 cells. (**a**) EphB expression was analysed by Real-time RT-PCR in PC-3 cells transfected with either single or double siRNA oligonucleotides as shown underneath. Data are expressed as fold change with respect to control siRNA treated cells. Values are means ± s.d. (n=3). (**b**) Lysates of PC-3 cells transfected with siRNA oligonucleotides (two different siRNA oligonucleotides, 1 and 2, were used to silence both EphB3 and EphB4) or transfected with a non-targeting siRNA oligonucleotide (control siRNA), were immunoblotted as shown. (**c**) PC-3 cells transfected with siRNAs as indicated and treated with clustered ephrin-B2/Fc or Fc for 20 min, were analysed for the formation of filopodia. Data are expressed as mean number of filopodia per cell ± s.d. (n=3, 50 cells counted per experiment) *** $p<0.001$, determined by an unpaired students t-test. (**d**) Confocal images of PC-3s transfected with siRNAs as indicated and treated with clustered ephrin-B2/Fc or Fc for 20 min, fixed and stained with phalloidin. Scale bar = 20 μm. (**e**) PC-3 cells transfected with siRNAs as indicated were added to transwell chambers coated with ephrin-B1/Fc and numbers of cells migrating through were scored. Data are expressed as fold change with respect to control Fc coated chambers (red dotted line). Values are means ± s.d. (n=3). * $p<0.05$, determined by an unpaired students t-test.

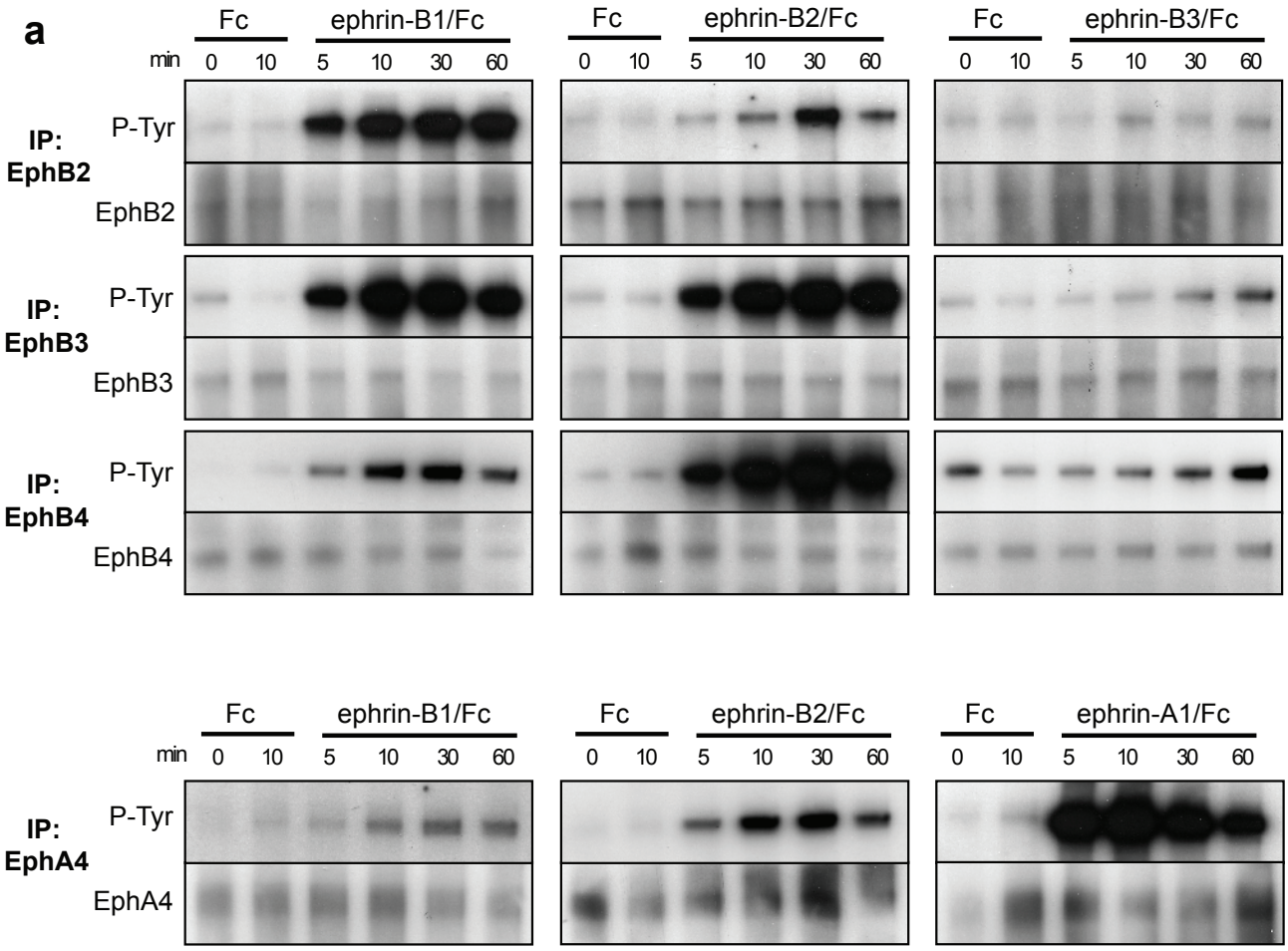

Figure S5 Activation of Eph receptors by ephrin ligands. (**a**) EphB2, B3, B4 and A4 were immunoprecipitated from lysates of PC-3 cells treated with ephrin ligands or Fc and immunoblotted for phosphotyrosine and total Eph receptor. Similar exposure times were used for each immunoblot.

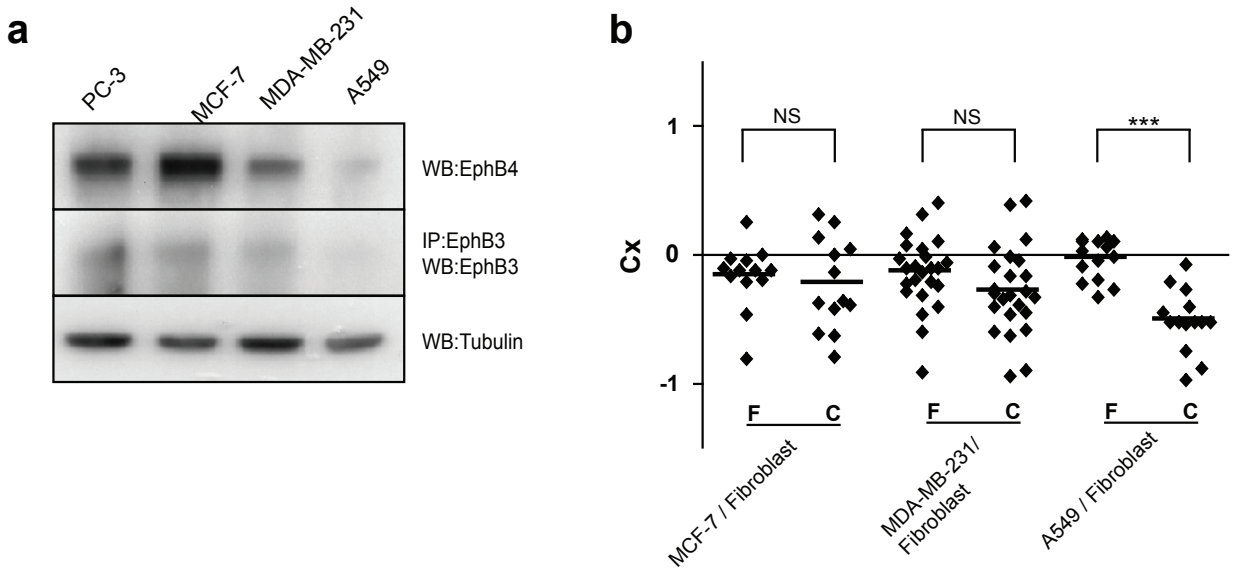

Figure S6 Cancer cell lines expressing EphB3/B4 fail to display heterotypic CIL. (**a**) EphB4 was immunoblotted and EphB3 was immunoprecipitated and immunoblotted from lysates of PC-3, MCF-7, MDA-MB-231 and A549 cells. (**b**) Contact acceleration indices (Cx) of free moving (F) versus collisions between cancer cells and fibroblasts (C). MCF-7 (n=13), MDA-MB-231 (n=24), A549 (n=14). ***p< 0.001, NS = not significant, determined by a Mann-Whitney test.

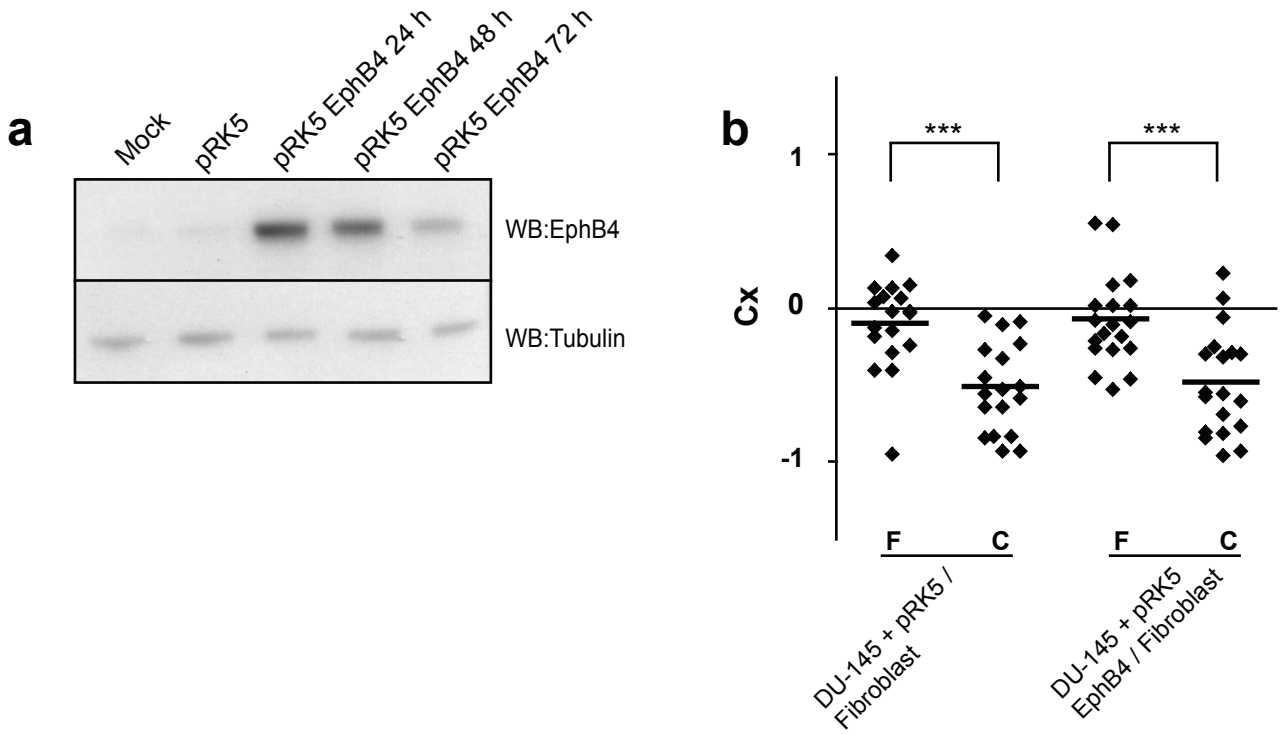

Figure S7 Expression of EphB4 in DU-145 cells is not sufficient to disrupt heterotypic CIL. (**a**) Lysates of DU-145 cells transfected with either pRK5, pRK5 EphB4 or no vector (Mock) for various times as indicated, were immunoblotted for EphB4 as shown. (**b**) Contact acceleration indices (Cx) of free moving (F) versus collisions between transfected DU-145 cells and fibroblasts (C). Cells were imaged between 48-72 h post-transfection. pRK5 (n=18), pRK5 EphB4 (n=19), ***$p < 0.001$, determined by a Mann-Whitney test.

Fig. 3a

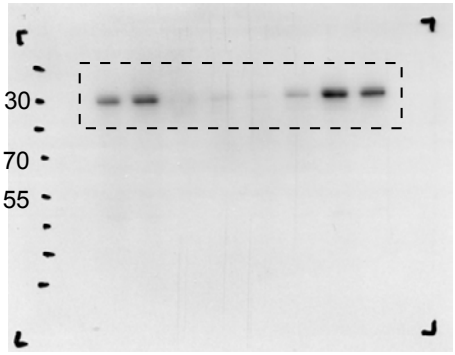

WB: EphA2

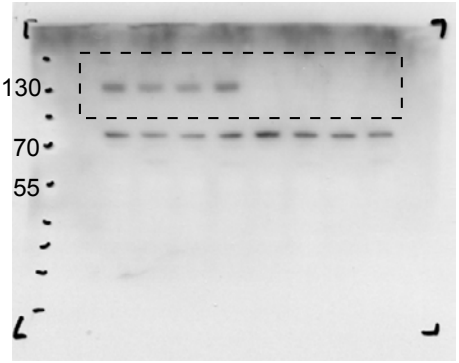

WB: EphA4

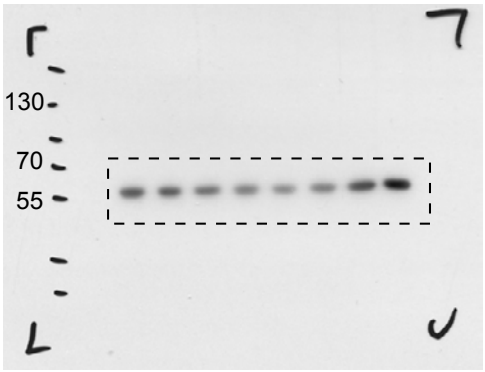

WB: Tubulin

Fig. 4b

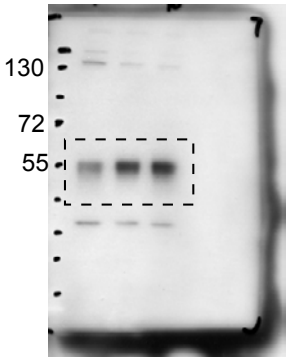

WB: ephrin-B2

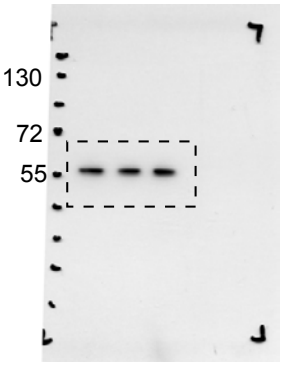

WB: Tubulin

Figure S8 Full scanned images of Western Blots. Molecular weights given in kDa.

Fig. 4d

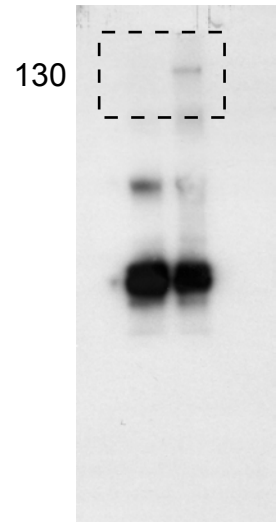

IP: EphB2
WB: EphB2

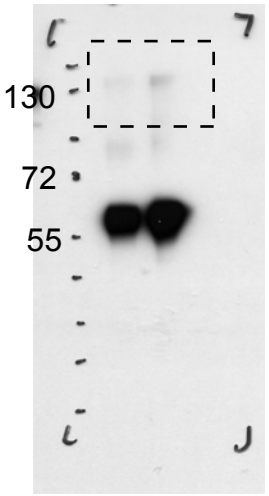

IP: EphB3
WB: EphB3

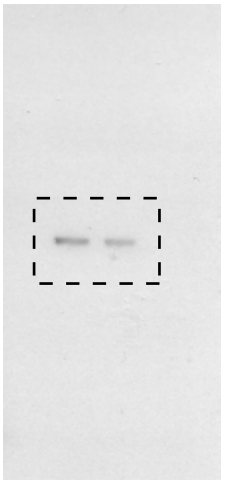

WB: Tubulin

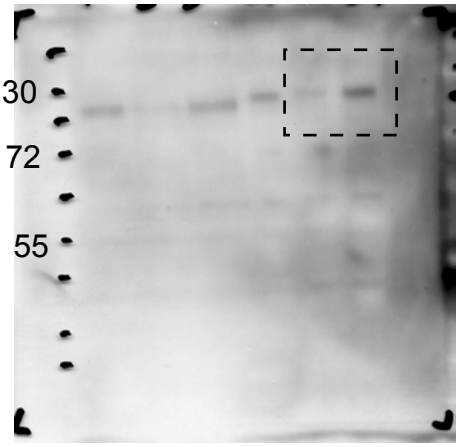

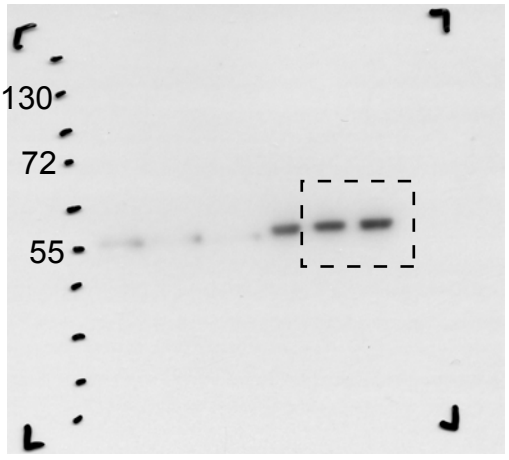

WB: Tubulin

Figure S8 continued

Fig. 5e

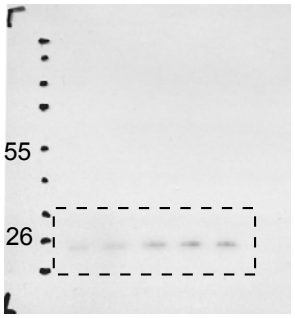

Pulldown Cdc42-GTP
WB: Cdc42

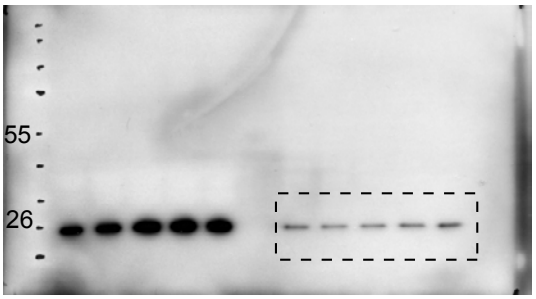

Lysates
WB: Cdc42

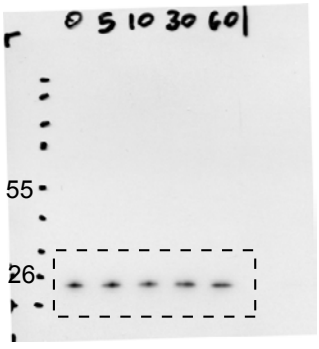

Pulldown Rac-GTP
WB: Rac

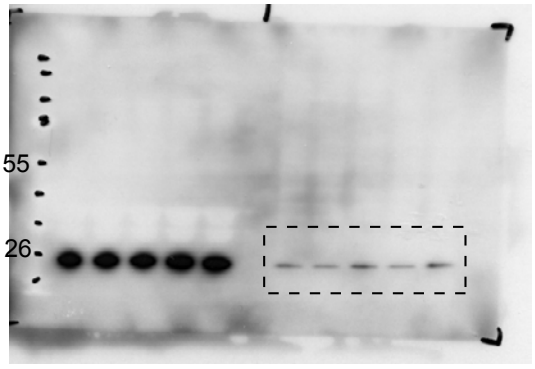

Lysates
WB: Rac

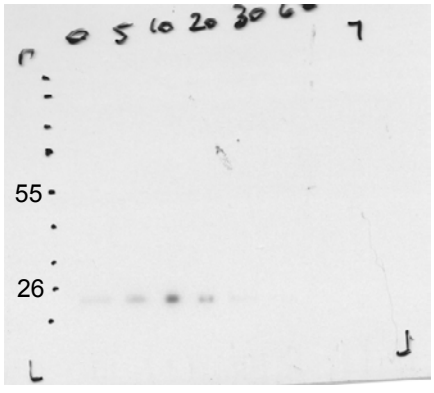

Pulldown Rho-GTP
WB: Rho

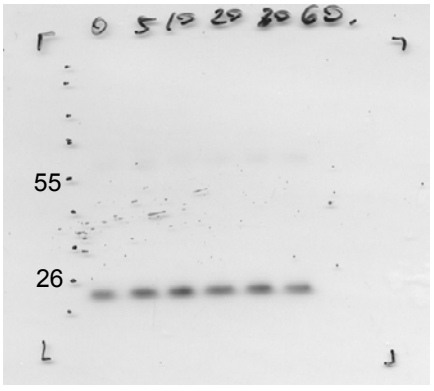

Lysates
WB: Rho

Figure S8 continued

Fig. 5g

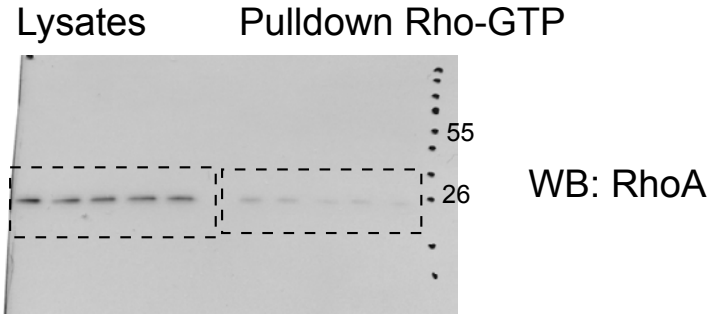

Fig. 6b

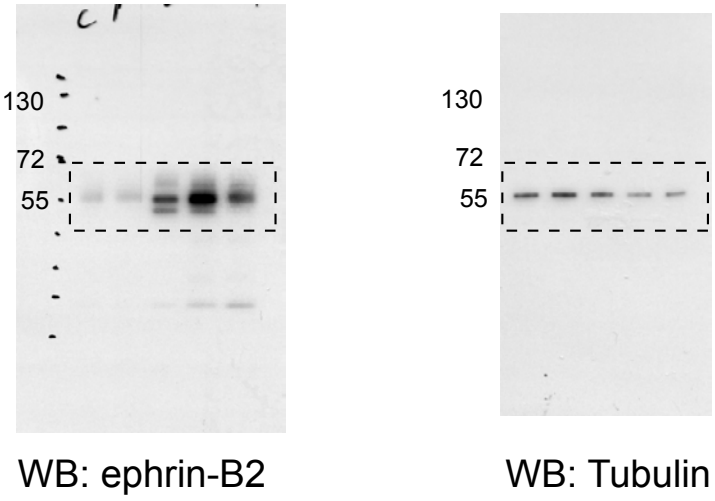

Fig. 6d

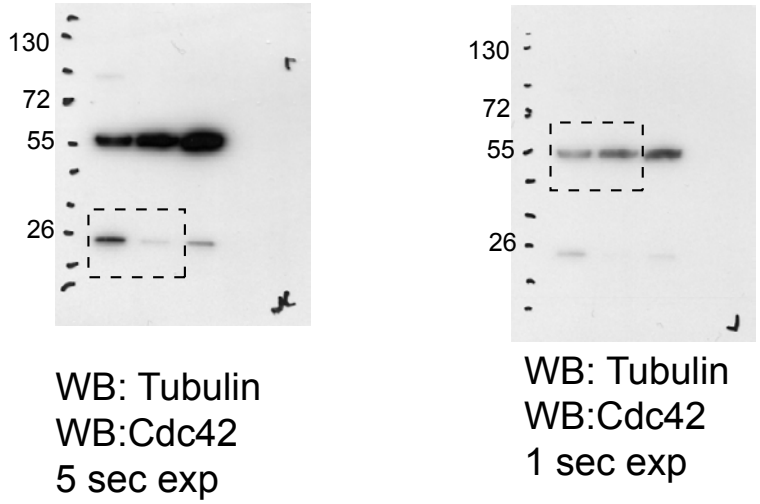

Figure S8 continued

Supplementary Fig. 2a

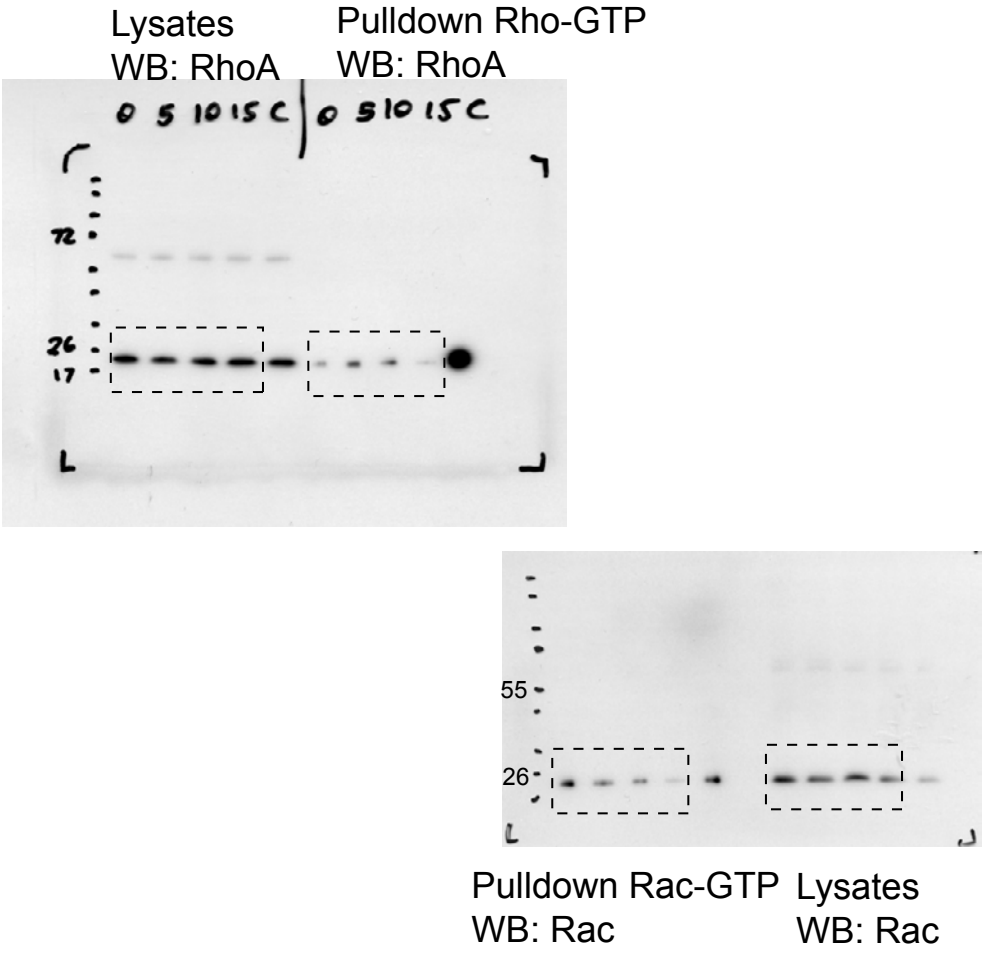

Figure S8 continued

Supplementary Fig. 4

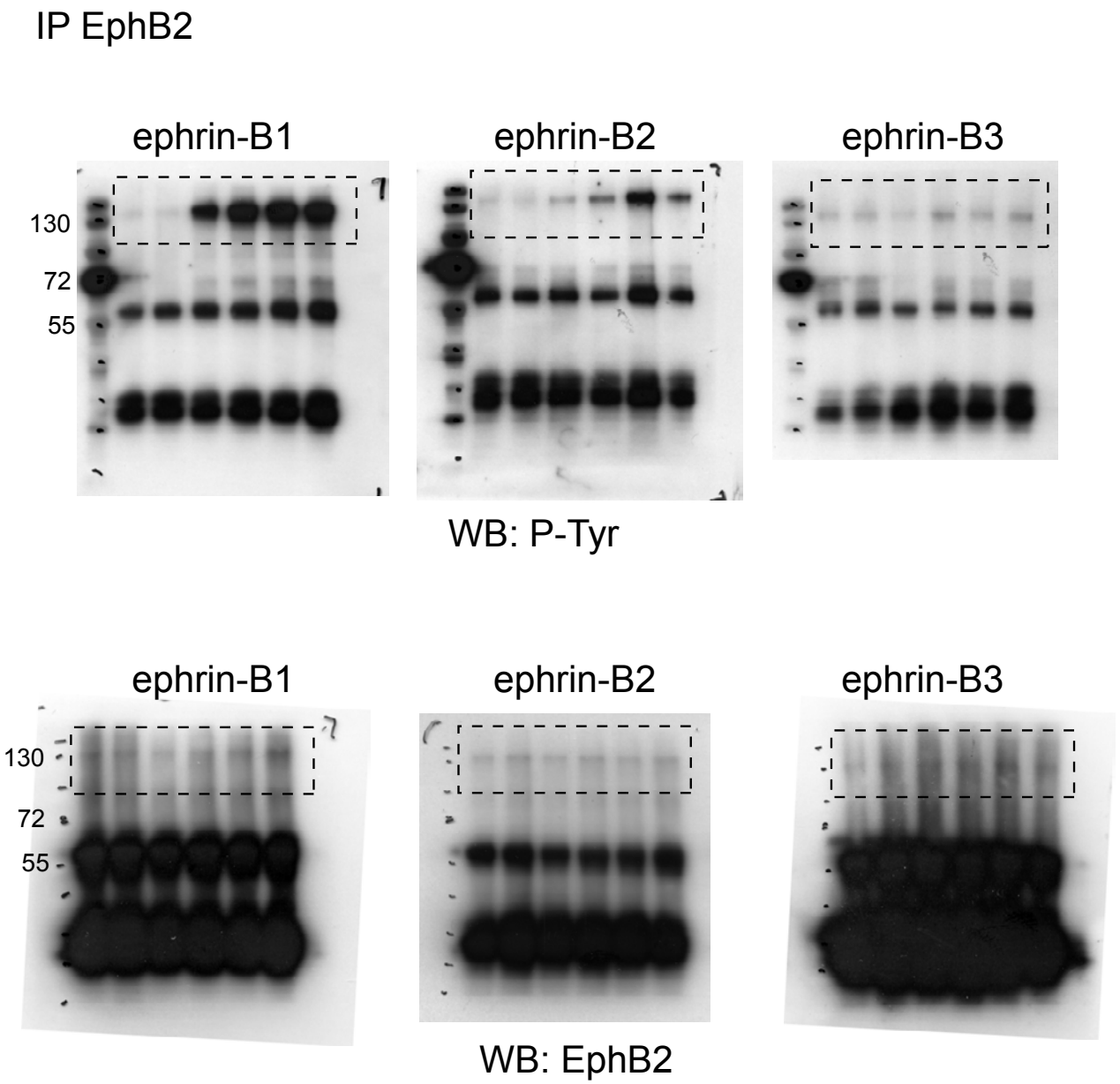

Figure S8 continued

Supplementary Fig. 4

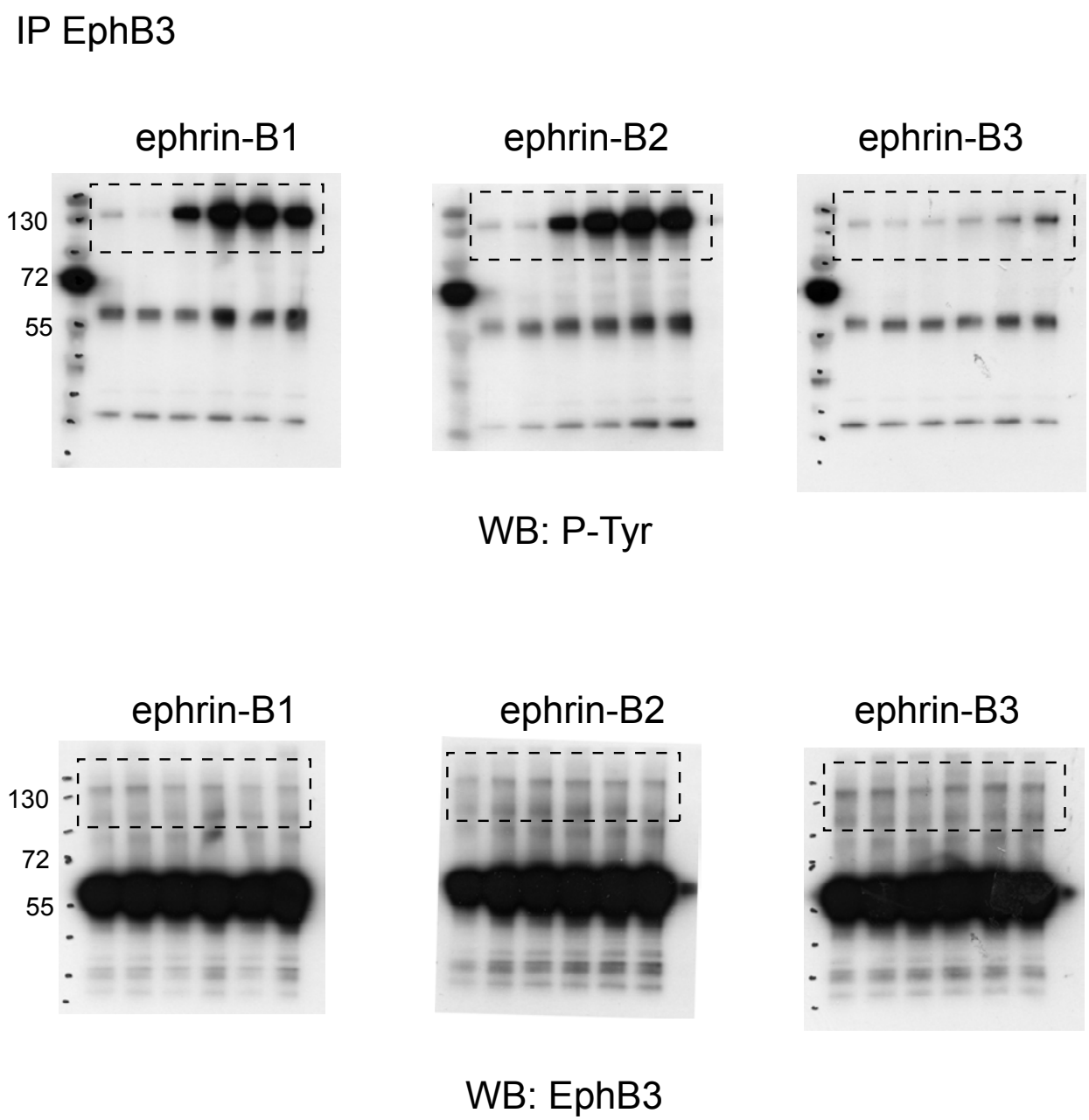

Figure S8 continued

Supplementary Fig. 4

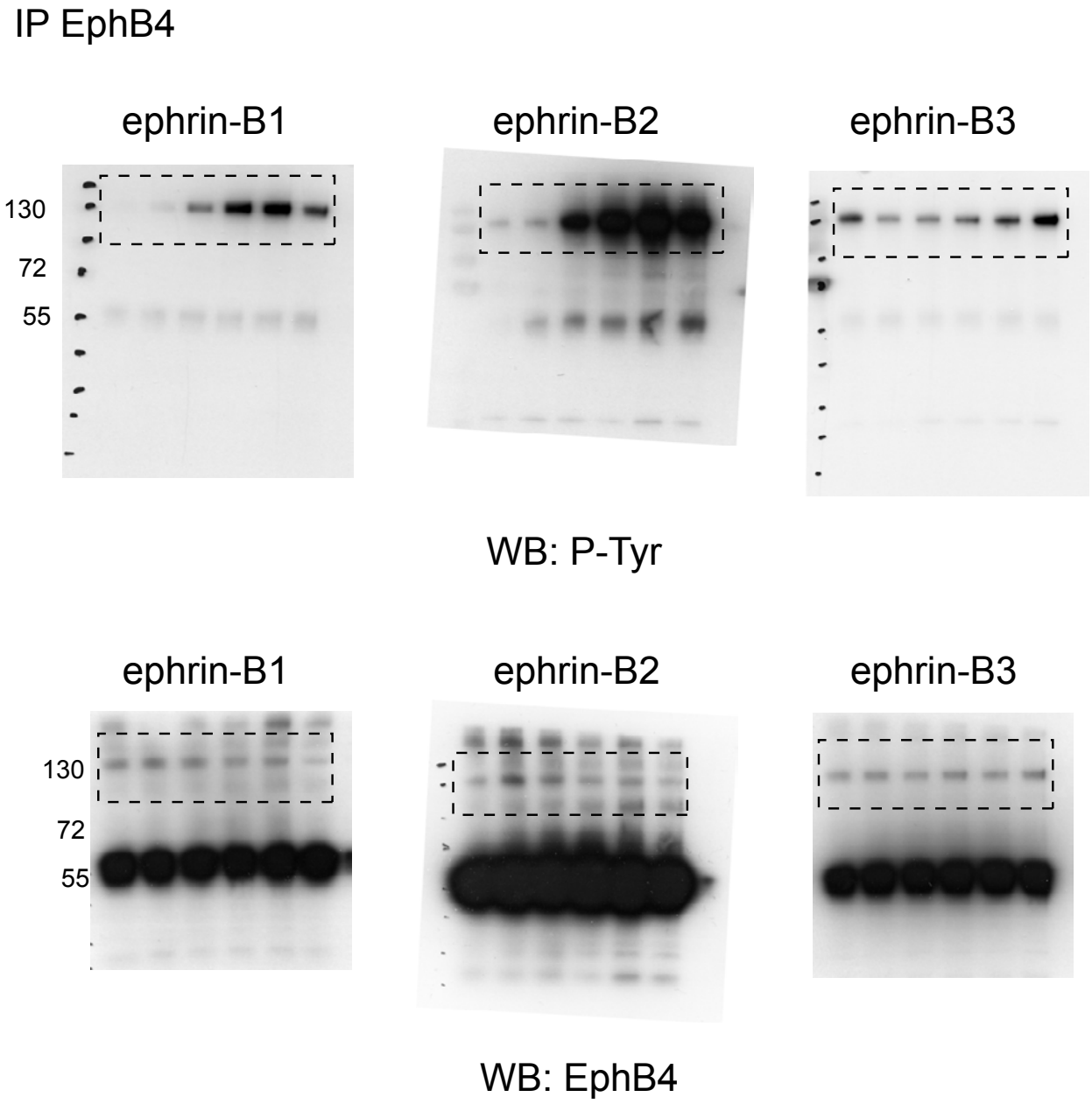

Figure S8 continued

Supplementary Fig. 4

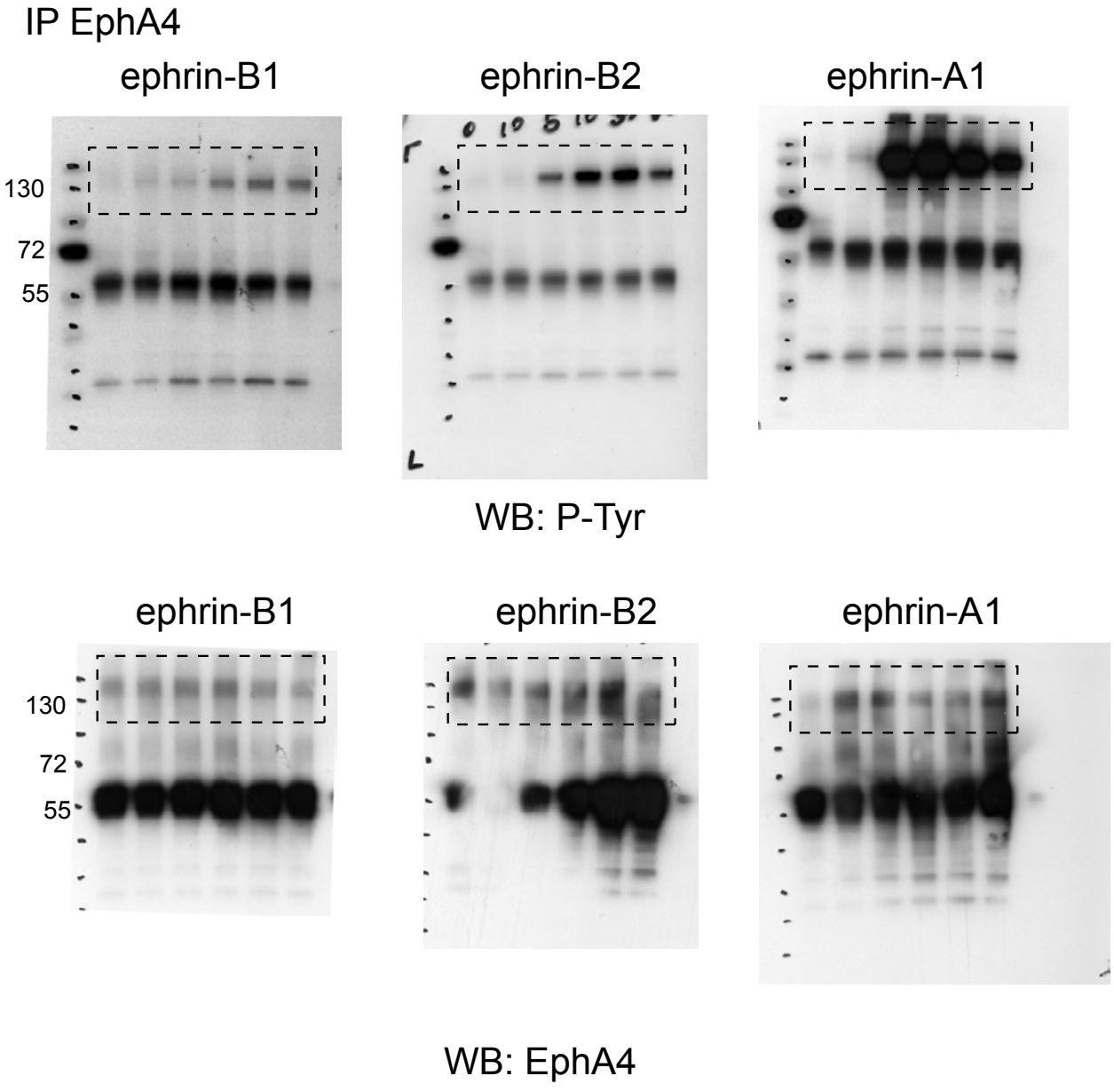

Figure S8 continued

Supplementary Fig. 5b

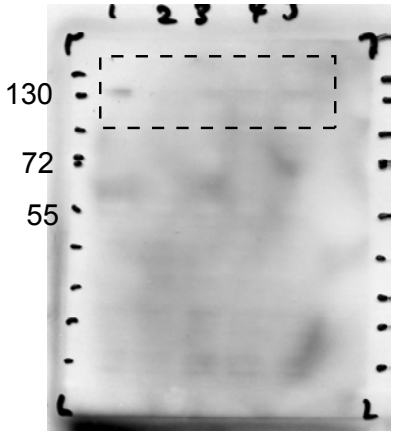

WB: EphB4

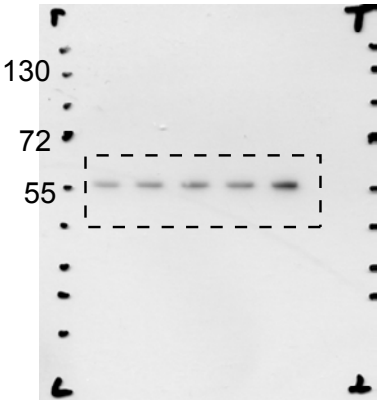

WB: Tubulin

55

Supplementary Fig. 6a

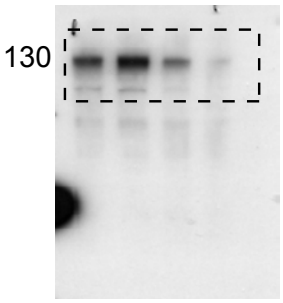

WB: EphB4

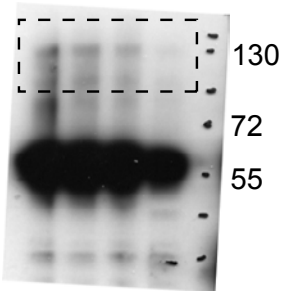

IP:EphB3
WB: EphB3

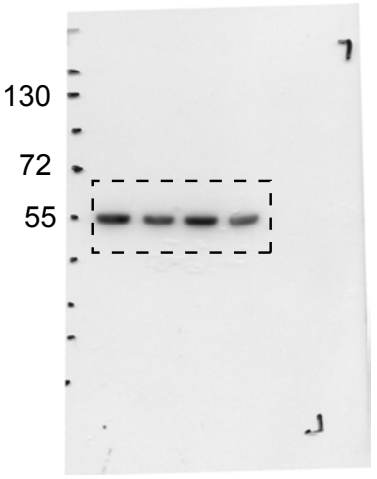

WB: Tubulin

Figure S8 continued

Supplementary Fig. 7a

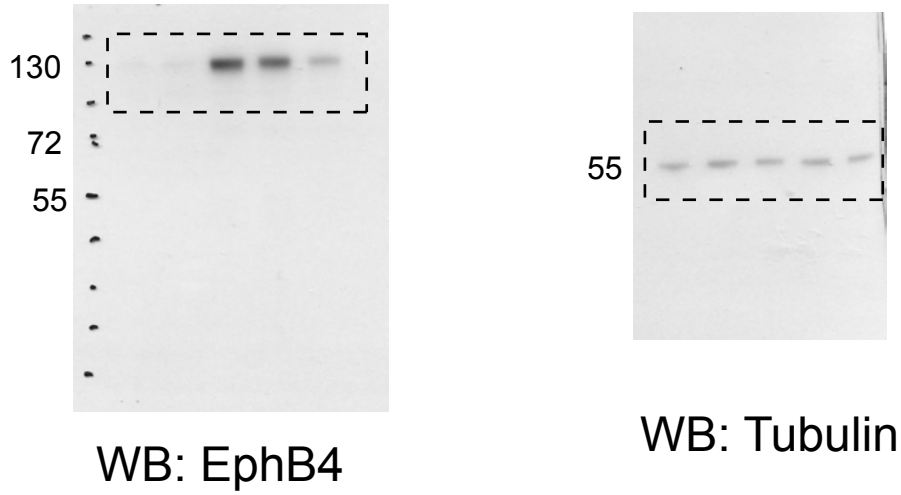

Figure S8 continued

Supplementary movie legends

Movie S1 PrEC and fibroblast heterotypic collision. Phase time-lapse images of a PrEC/fibroblast collision. Frames taken every 15 sec for 32 min and displayed at 12 fps.

Movie S2. PC-3 and fibroblast heterotypic collision. Phase time-lapse images of a PC-3/fibroblast collision. Frames taken every 15 sec for 180 min and displayed at 12 fps.

Movie S3 PrEC homotypic collision. Phase time-lapse images of two PrEC cells colliding. Frames taken every 15 sec for 45 min and displayed at 12 fps.

Movie S4 PC-3 homotypic collision. Phase time-lapse images of two PC-3 cells colliding. Frames taken every 15 sec for 45 min and displayed at 12 fps.

Movie S5 PC-3 colliding with ephrin-A5/Fc coated silica bead.
Phase time-lapse images of a PC-3 cell colliding with an ephrin-A5/Fc coated bead. Frames taken every 15 sec for 60 min and displayed at 12 fps.

Movie S6 PC-3 colliding with /Fc coated silica bead. Phase time-lapse images of a PC-3 cell colliding with an Fc coated bead. Frames taken every 15 sec for 53 min and displayed at 12 fps.

Movie S7 Homotypic collision between control siRNA PC-3 cells. Phase time-lapse images of two control siRNA treated PC-3 cells colliding. Frames taken every 15 sec for 51.5 min and displayed at 12 fps.

Movie S8 Homotypic collision between EphA2/A4 siRNA PC-3 cells. Phase time-lapse images of two EphA2/A4 double siRNA knockdown PC-3 cells colliding. Frames taken every 15 sec for 105 min and displayed at 12 fps.

Movie S9 PC-3 cells treated with clustered ephrin-B2/Fc. Phase time-lapse images of PC-3 cells treated with 1ug/ml of ephrin-B2/Fc preclustered with 10ug/ml of anti-Fc antibody. Ephrin-B2 addition corresponds to the white frame. Frames taken every 15 sec for 50 min and displayed at 12 fps.

Movie S10 Heterotypic collision between control siRNA PC-3 cell and fibroblast. Phase time-lapse images of a control siRNA knockdown PC-3 cell colliding with a fibroblast. Frames taken every 15 sec for 75 min and displayed at 12 fps.

Movie S11 Heterotypic collision between EphB3/B4 siRNA PC-3 cell and fibroblast. Phase time-lapse images of an EphB3/B4 double siRNA knockdown PC-3 cell colliding with a fibroblast. Frames taken every 15 sec for 75 min and displayed at 12 fps.

Supplementary Information, Table 1

Primers used in this study:

Gene	siRNA Sequence	Catalogue number
EphA2-1	UGA AUG ACA UGC CGA UCU A	J-003116-09
EphA2-2	GAA GUU CAC UAC CGA GAU C	J-003116-10
EphA4-1	GAA CUU GGG UGG AUA GCA A	J-003118-09
EphA4-2	GCA AUU GCC UAU CGU AAA U	J-003118-10
EphB2	CAC GAC ACG UCA CCA AGA A	J-003122-13
EphB3-1	UCA ACG GUG UCU CGG GCA A	J-003123-17
EphB3-2	GGA AGU GUG CCG UGG UCG A	J-003123-19
EphB4-1	GUA CUA AGG UCU ACA UCG A	J-003124-09
EphB4-2	GGA CAA ACA CGG ACA GUA U	J-003124-10
EphB6	GGC AAA GUC UAU UUC CAG A	J-003125-09
Cdc42	CGG AAU AUG UAC CGA CUG U	J-005057-05
Non-target Control	UGG UUU ACA UGU CGA CUA A	D-001810-01

Gene	Forward Primer	Reverse Primer
EphA1	AGACCTTAAAAGACACATCCCC	ACCTCCCACATCACAATCCC
EphA2	TTGGCTTCTTTATCCACCGC	TTGTACACCTCCCCAAACTC
EphA3	ATGTTTCCAGACACGGTACC	CCATCTTCCTGAGTAGAACTGTGAGG
EphA4	ACAGACAAACAGAGGAGAGAC	CCAGATCACGATGCACATAG
EphA5	CCTTCTGTGGTACGACACTTG	GGTCTGCACACTTGACAGGTG
EphA6	AGGAAGCTGGGGCAAAACGCCTCCAC	CCGCTGTTGGCGGATTCACTC
EphA7	TCAACATCAACCAAACCACAG	CCATAACCAGCAGCAGTAAAAG
EphA8	ATGGAGGTGGAGACCGGGAAAC	TGATGCAGAGGCAGGAAGACAG
EphA10	CCAAGTGTGCCCTGACTACCTGTC	GTTCAGCCAAAGAGATGCCTAGGCTCAC
EphB1*	TTCACTTCAGCCAGCGAC	TTTCCCTCCTCTCCTTCCC
EphB2*	ATGGCGCCCCTCTCCTCTGGCATCA	ACCGCTTGGTTCTTCCCGTG
EphB3	GCATCGCCTCCACAGTGACC	ACGAAGACAAGCCCAGCTGTA
EphB4	TTCGGCCAGGAACATCACAG	CCGATGAGATACTGTCCGTG
EphB6	TACCTGTCCAGCTTTGCC	TCTCCATAACTCATCACTTCCC
EfnA1	CGGAATGAGGACTACACCATACATGTGCAGC	AAGCAGCGGTCTTCATGCTGGTGGATGGGTT
EfnA2	CTACACGGTGGAGGTGAGCA	ACAGCATTGGGAGGCGTGGCA
EfnA3*	ACTACATCTCCACGCCCAC	TCCCGCTGATGCTCTTCTC
EfnA4*	TTGTACATGGTGGACTGGCC	AGAACTCTCTGGAGTGGGCACC
EfnA5	CCAGAAGATAAGACTGAGCGC	CCATTATCTGGGATTGCAGAGG
EfnB1	CCAATGCTGTGACGCCTGAG	CGAACAATGCCACCTTGGAGTTG
EfnB2	GGAAGAAGTTCGACAACAAGTCC	TTCAGCAAGAGGACCACCAGCGT
EfnB3	TGGAGCCTGGGAAGGAGAACC	CAGGGTGGCGACTCTCCGAAG

* For Real-Time RT-PCR of these genes QuantiTect Primer Assays (Qiagen) were used.

Gene	QuantiTect Primer Assay
18S RNA	QT00199367
EphB1	QT00019327
EphB2	QT00089495
EfnA3	QT00091770
EfnA4	QT00063028

Antibody Dilutions:

Antibody	Western Blotting	Immunostaining
Anti EphA2	1:1000	-
Anti EphA4	1:5000	-
Anti EphB2	1:750	-
Anti EphB3	1:2500	-
Anti EphB4 (C- terminal)	1:1000	1:100
Anti EphB4 (N-terminal)	-	1:50
Anti ephrinB2	1:2000	1:100
Anti fascin		1:50 (methanol fixed)
Anti RhoA	1:750	-
Anti Rac	1:1000	-
Anti Cdc42	1:1000	-
Anti alpha tubulin	1:5000	-